U.S. Department of Commerce
National Oceanic and Atmospheric Administration
National Weather Service
National Centers for Environmental Prediction
5830 University Research Court College Park, MD 20740

NCEP Office Note 491

https://doi.org/10.7289/V5/ON-NCEP-491

Improving Surface Wind Databases for Extreme Wind-Wave Simulation and Analysis in the South Atlantic Ocean

Jose-Henrique G. M. Alves[i]
Systems Research Group Inc at the US National Centers for Environmental Prediction
EMC/NCEP/NOAA, College Park, MD, USA

Ricardo M. Campos, Carlos Guedes Soares
Centre for Marine Technology and Ocean Engineering (CENTEC), Instituto Superior Técnico,
Universidade de Lisboa, Portugal
Programa de Engenharia Oceânica COPPE, Universidade Federal do Rio de Janeiro, RJ, Brazil

Carlos E. Parente
Programa de Engenharia Oceânica COPPE, Universidade Federal do Rio de Janeiro, RJ, Brazil

Oct 31, 2017

This is an internal-reviewed manuscript, primarily intended for informal exchange of information among the ncep staff members.

MMAB Contribution 332

[i] Corresponding Author, e-mail address: henrique.alves@noaa.gov

ABSTRACT

An investigation is made of the quality of a publicly available atmospheric reanalysis as potential sources for winds driving wind-wave hindcasts, focusing on extreme sea state applications in the South Atlantic Ocean, namely the Climate Forecast System Reanalysis (CFSR/NCEP). Significant CFSR surface wind biases are found relative to buoy and satellite measurements, particularly in upper-percentiles. Two different approaches for calibration of the CFSR wind data are presented and compared. One applies a simple linear regression model, with coefficients obtained from the comparison of CFSR against buoy data. The second is a method where deficiencies of the CFSR associated with severe sea state events are remedied, whereby "defective" winds are replaced with satellite data within cyclones. Linear regression generally increases in around 5% to 6% CFSR wind intensities. However, the process still retains an underestimation by CFSR of up to 25% of remotely-sensed winds within strong extra-tropical storms. Under intense cyclonic conditions, the proposed method of blending satellite-derived cyclonic wind fields with background CFSR data proves effective, leading to a better representation of winds both during ambient or extreme conditions. Six alternative wind data sets are built to force the wave model WAVEWATCH III, focusing on the South Atlantic. Assessment of results points to a significant advantage of combining both CFSR wind adjustment methods, which jointly produce high-quality winds with benefits for wave hindcasts and general applications including extreme wave analysis.

Keywords: wind reanalysis; extreme analysis; wind-wave hindcasts; cyclones; wind calibration; South Atlantic Ocean.

1. Introduction

Coastal regions in several South American countries are exposed to extra-tropical and sub-tropical cyclones occurring in the South Atlantic Ocean, which can pack strong winds leading to marine and coastal hazards. Fortunately, most cyclone tracks involving extreme systems do not hit these regions directly. However, the oceanographic effect of the southerly fetches and cold fronts in the western part of the ocean result in extreme events of combined storm surge and wind-waves. Many losses and accidents are reported every autumn and winter in shorelines exposed to the South Atlantic, due to the effect of extreme waves and surges. Thus, the proper representation of extreme winds associated with cyclones in the South Atlantic Ocean is a key effort to improve short-term forecasts and warnings, as well as long-term extreme analysis for met-ocean design criteria in that ocean basin.

The current work proposes an approach to construct a database consisting of improved surface wind speeds for ocean modeling applications, focusing on cyclonic conditions with potential to generate severe marine weather conditions in the South Atlantic Ocean. The approach developed in this study has provided the foundation to the development of a wave hindcast and extreme wave analysis database described in Campos et al (2017). Data used presently are obtained from the Climate Forecast System Reanalysis (CFSR; Saha et al., 2010), based on selection criteria discussed below.

The improved wind database is achieved via the application of two methods of wind calibration using buoy measurements and satellite data, which are discussed and compared. The methodology is implemented to surface winds at the 10-meter height only, which is the target variable in this present paper, as this is the primary parameter driving wind-waves and surges. Campos et al. (2017) addresses the construction of a wave hindcast database built using the state-of-the-art wind-wave model WAVEWATCH III (Tolman et al., 2014) and the wind fields developed presently.

Winds, waves and currents are the most important environmental loads that act on ships and offshore structures (Bitner-Gregersen et al., 2015). Historically, this concern led the Brazilian Navy, alongside universities and the Brazilian Oil Company PETROBRAS, to increase the amount of observations made in the south and southeastern Brazilian regions. There, due to a much larger scale of offshore operations relative to other parts of the country, information about the local metocean climate is relatively more abundant. Taking advantage of the relative wealth of data in those regions, Souza (1988) and Parente and Souza (1989) made initial studies about the climatology of sea states in Campos Basin (offshore waters in the north of Rio de Janeiro). Their results described the persistence of wind seas and mid-frequency waves coming from northeast, generated by the semi-permanent South Atlantic anticyclone, occurring together with swells coming from south that were occasionally associated with much higher waves. Other studies, such as Alves (1996) confirmed that similar wave climate patterns also occurred in the southern coast of Brazil.

Hence, in the late 80's and early 90's, the bi-modal nature of the local wave climate in south and south-eastern Brazil was outlined and started to be intensively studied. Parente (1999) developed a new technique to process heave-pitch-roll wave buoys, named Directional Analysis with Adaptive Techniques (DAAT), which allows accurate estimations of direction and energy of different wave groups coexisting in the same frequency. It made possible the investigation of separate sea states generated by different meteorological systems occurring in the same location. Such interest led to several other studies since the late 90's, which have contributed to the knowledge about the wind and wave climate offshore the south and southeastern coasts of Brazil.

Parente (1999) followed by Pinho (2003) propose dividing the wave climate in southeastern Brazil into four categories:

1. "Bom Tempo" (good weather) with swell;
2. "Bom Tempo" (good weather) without swell;
3. "Mau Tempo" (bad weather) with storm winds from southwest;
4. "Mau Tempo" (bad weather) with storm winds from southeast.

Categories 1 and 2 are found when the large sub-tropical anticyclone is dominant, with light to moderate winds from northeast, normally associated with clear sky and small waves in high frequencies – up to 2.5 meters of height and 6 seconds of period. They represent the most common condition in the large coasts of Sao Paulo, Rio de Janeiro and Espirito Santo states. Occasionally, swells generated by distant cyclones in southern latitudes propagate towards Brazil with high periods and sometimes high waves; this condition represents a major threat to ships and offshore structures due to the highly energetic bimodal sea state. Accurate forecasts under these conditions are extremely important, but are considered a great challenge due to the complex wave generation process involving many meteorological systems, some of them very far from Brazil, and to the lack of in-situ measurements that could assist a proper analysis of atmospheric conditions.

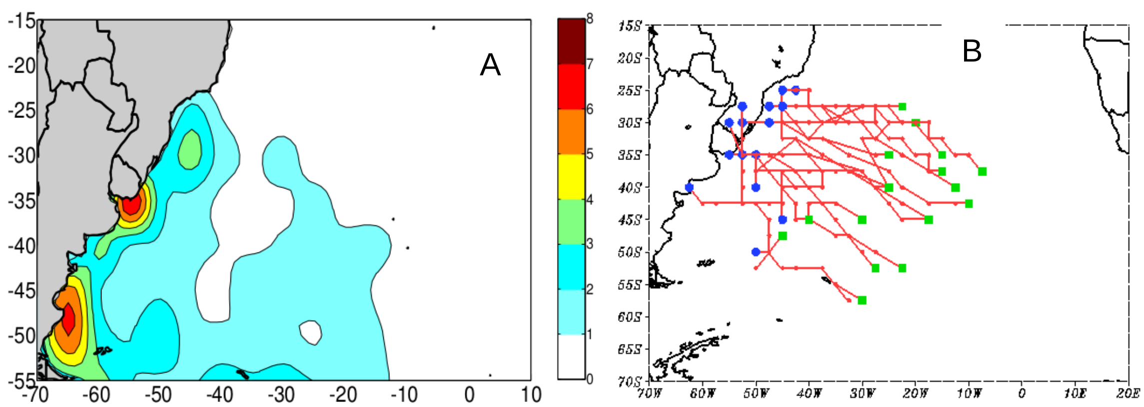

Figure 1 Main cyclogenesis areas extracted from Reboita (2008) on the left and cyclone tracks associated with extreme waves in southeastern Brazil extracted from Campos (2009) on the right. Both studies are based on NCEP/NOAA reanalysis-1 winds (Kalnay et al., 1996).

Categories 3 and 4 are associated with cold fronts, cloudy and rainy weather and strong winds from low pressure systems. The south and southwest winds and waves compose the most extreme conditions; the highest waves are those generated by cyclones at mid-latitudes with positions discussed by Campos et al. (2012) and Dragani et al. (2013), illustrated in Figure 1. Although winds and waves from the southeast and east are not associated with the highest extremes, the coastline orientation makes this family of events an important threat to several major states in the southeastern and southern Brazilian seaboard, including Rio de Janeiro (Godoi et al., 2014), Rio Grande do Sul and Santa Catarina (Alves, 1996; Alves and Melo, 2001), extending into Uruguay and Argentina (Dragani et al., 2013; Alonso et al.,2015. Therefore, the severity of metocean extremes in Brazil are dependent on the position of fetches and cyclone tracks, as discussed by Alves (1996) and Campos et al. (2012) in terms of wave heights, and by Campos et al. (2010) in terms of storm surges.

A description of the main cyclonegetic areas in the Southwest Atlantic Ocean, and of the cyclone tracks associated with highest waves are provided in several previous studies (e.g., Gan and Rao, 1991; Sugahara, 2000; Reboita, 2008). Figure 1 presents some results from Reboita et al. (2009) and Campos (2009), summarizing the identification of a significantly large oceanic area in the South Atlantic where surface winds are sufficiently strong to generate extreme waves offshore of south and southeastern coasts of Brazil.

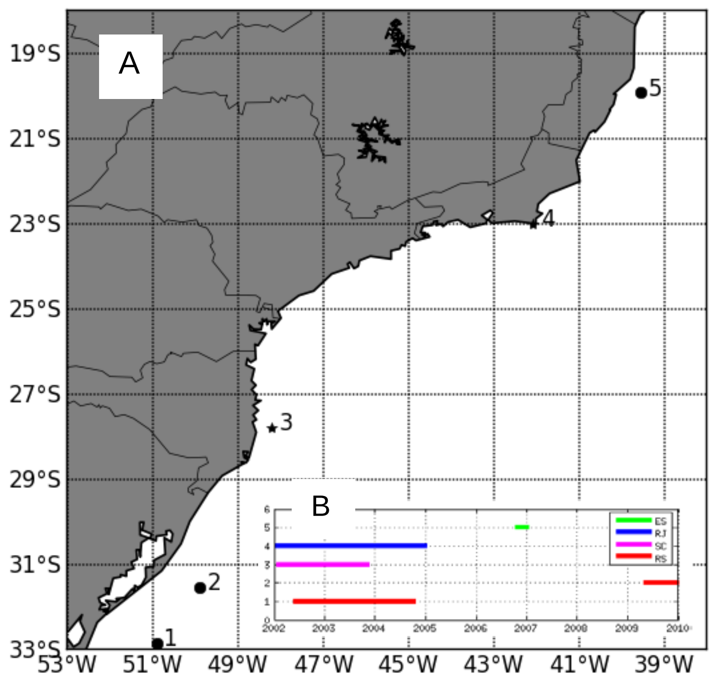

Figure 2 - Buoy locations (A) and duration of available measurements (B). Rio Grande do Sul (RS), Santa Catarina (SC), Rio de Janeiro (RJ) and Espirito Santo (ES).

Considering the large swaths involved with wave generation in the area of interest to our investigation, and the poor coverage by *in situ* platforms in Brazil, the use of satellite data became an important source of data in the present study. Despite the heavy dependence on remotely-sensed data, a limited number of buoys was used to provide "ground truth" in this study. Figure 2 illustrates buoy measurement sites selected for this paper. Data from other buoys were provided by private companies in the oil & gas industry with restrictions (e.g., only information of some extreme events were retained). Despite the limited data set provided by such buoys, they provide an important source of data to evaluate both numerical model and satellite data. In addition to measuring waves, buoys (1), (2) and (5) carried meteorological instruments and provided wind data and other atmospheric variables that were presently (see, e.g. section 3).

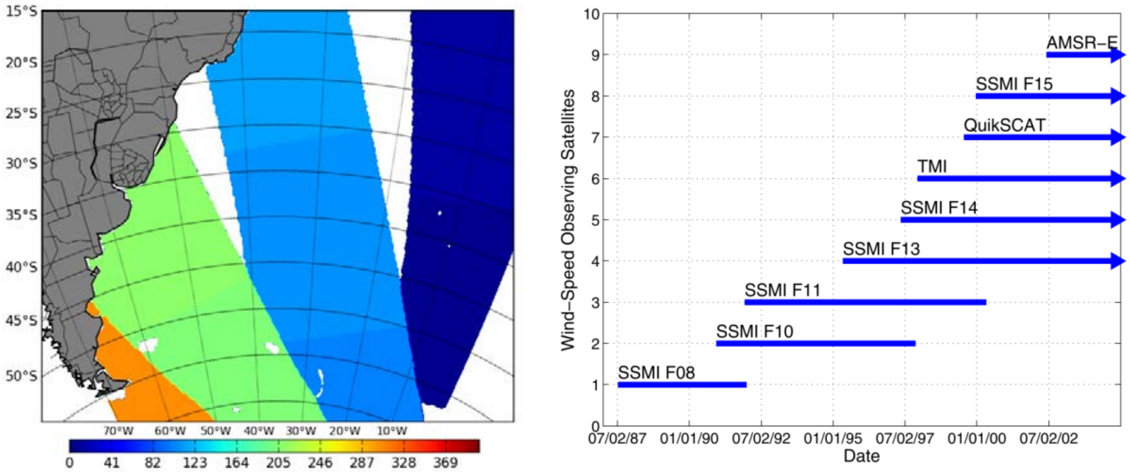

Figure 3 QuikSCAT satellite track, with colors and representing different swaths in hours (left). Additional scatterometer missions and durations (from Zhang et al., 2006; right).

The available remotely-sensed wind data used here, as well as the duration of the associated satellite missions are shown in Figure 3. Relative to previous decades, the amount of satellite observations has significantly increased since the early 2000’s. The left panel in Figure 3 illustrates the passage of QuikSCAT (JPL, 2001) within the region of interest. It is important to note some gaps between satellite passages as well as the time interval between tracks. This represents a great challenge when using satellite data to investigate the evolution of cyclones that have quick generation and displacement, especially when associated with extreme events. Therefore, using only the QuikSCAT data would be insufficient to properly describe cyclones, and a larger data source of remotely-sensed winds was sought after and found within the SeaWinds (NCDC/NOAA; Zhang et al., 2006) database. Coverage provided by the latter is seen in Figure 3 from data available at nomads.ncdc.noaa.gov/data/seawinds/uv/6hrly/netcdf/. SeaWinds data are used in association with QuikSCAT data in the present study to evaluate and calibrate the CFSR reanalysis, as described below.

2. The CFSR surface winds reanalysis

The common problem of lack of in-situ measurements increases importance of weather and climate reanalyses in several engineering applications. The problem is more critical for ocean sciences in the Southern Hemisphere basins, where measurements are much scarcer than other basins in the Northern Hemisphere. In the former regions, the lack of observations, nevertheless, reduces the quality of reanalyses, affecting therefore using its data as forcing in wind-wave hindcasts. The present study proposes an effective approach towards solving the latter problem, namely the application of wind-wave hindcasts forced with corrected reanalyses from the US National Centers for Environmental Prediction (NCEP), focusing on extreme wave analysis in the South Atlantic Ocean basin.

Corrections made to improve the quality of wind reanalyses consist of simple linear regression adjustments, associated with the use of measurements to improve extreme cyclonic winds near the ocean surface, where measured data is not necessarily assimilated with appropriate weight. The latter approach is not new, and has been implemented in previous studies, including Powell et al. (2010), who used a large number of observations to reconstruct the surface winds of Hurricane Katrina. However, applications of surface wind corrections within cyclones on a global or basin-wide scales for the purposes of generating wave hindcasts has not been widely explored.

NCEP and the European Center for Medium-Range Weather Forecast (ECMWF) have been producing state-of-the-art reanalysis products for the last three decades (Kalnay et al., 1996; Kistler et al., 2001; Gibson et al., 1997; Uppala et al., 2005; Dee et al., 2011). The most recent NCEP reanalysis database was generated as part of the Climate Forecast System Reanalysis project (CFSR, Saha et al, 2010). The CFSR reanalysis is a global product covering the period 1979 to 2009 in its first release. The wind fields have resolution of 18.5' (~0.31°) and 1 hour, but are distributed in a ½° global grid. The CFSR reanalysis uses the NCEP atmospheric Global Forecast System (GFS) with a robust data assimilation system. A detailed description is provided in Saha et al. (2010). CFSR data is freely available to the public[2].

Stopa and Cheung (2014) evaluated the flagship reanalyses from NCEP and ECMWF, CFSR and ERA-Interim, respectively. They pointed at some discontinuities in the CFSR in the South Atlantic Ocean, which was confirmed in a recent application of the CFSR to wind-wave hindcasts (Chawla et al, 2013). In the context of the present study, Stopa and Cheung (2014) found important divergences between both NCEP and ECMWF reanalyses for the higher wind percentiles, mainly for the top 1% level. The authors conclude that both reanalyses underestimate extreme events above the 95% percentile. According to their results, ECMWF's ERA-Interim underestimates the upper percentile measurements by 8% on average, whereas NCEP's CFSR shows better agreement with observations, with an underestimation of 3% on average. This better agreement between CFSR and observed upper percentiles extends to the 99.8% mark, when the quality deteriorates significantly. Results of Stopa and Cheung (2014) were later confirmed by Campos and Guedes Soares (2016b) with an evaluation of CFSR and ERA-Interim

[2] http://nomads.ncdc.noaa.gov/data/cfsr/

using GlobWave satellite data; they confirmed the better performance of CFSR under severe wind conditions.

Among available surface winds from global reanalyses, the CFSR was selected for our study because of the availability of public data at higher spatial and temporal resolutions, and for its better performance at higher wind speed percentiles. The reasoning may be summarized as follows:

- Higher resolution: the focus of this paper is on extreme events and the spatial and temporal resolution is of great importance for the proper simulation of cyclones and extreme waves, as discussed by Cavaleri and Bertotti (2004), Cavaleri and Bertotti (2006) and Cavaleri et al. (2007);
- Performance of the higher percentiles: as described by Stopa and Cheung (2014), the CFSR surface winds are in better agreement with measurements under extreme events;
- Portability for operational applications: CFSR was produced with the GFS model, which is also used operationally at NCEP. Therefore, the methodology applied in the present study using a NCEP hindcast can be adopted and implemented for NCEP forecasts;
- Both CFSR and the operational GFS provide publicly available datasets, which favor usage and replication of the results reported presently by the public, which is not the case of ECMWF forecast products.

The next two sections evaluate CFSR 10-meter winds against buoy and satellite data. Only the wind intensity is analyzed. It is important to note that buoy data used for the assessment are independent – e.g., were not assimilated into the CFSR reanalysis; while QuikScat scatterometer data were assimilated into CFSR for the period from 2001 to 2009.

3. Evaluation of CFSR wind speeds relative to buoys

In-situ metocean data available for validation during the study period are limited to buoys 1, 2 and 5, shown in Figure 2. However, buoys 2 (N Rio Grande do Sul) and, especially, buoy 5 (Espirito Santo) have very limited duration. Buoy 1 (S Rio Grande do Sul), produced data for the period between 2002 and 2004. Therefore, it will be the main source of observations to evaluate CFSR winds. For reference, results for buoys 2 and 5 are also provided. Buoys 1 and 2 are Axys buoys with two anemometers at 3.7 and 4.7 meters, whereas buoy 5 is an experimental platform developed in Brazil with anemometer at 3.0 m height. In all cases, winds must be converted to the height of 10 meters, matching the CFSR data. For that purpose, we use the LKB method described by Liu et al. (1979), which corrects wind speeds using a logarithmic profile adjusted to atmospheric stability, taking into account the air and sea temperatures, atmospheric pressure and humidity – also measured at the buoys. All buoys considered each hourly wind as the 10-minutes average.

Validation statistics used henceforth for wind and wave parameters are: mean error (ME), correlation coefficient (CC), scatter index (SI) and root mean square error (RMSE) as follows.

$$ME = \frac{\sum_{i=1}^{n}(S_i - R_i)}{n} \quad (1)$$

$$RMSE = \sqrt{\frac{\sum_{i=1}^{n}(S_i - R_i)^2}{n}} \quad (2)$$

$$SI = \frac{RMSE}{\bar{S}} \quad (3)$$

$$CC = \frac{\sum_{i=1}^{n}(S_i - \bar{S})(R_i - \bar{R})}{\left(\sum_{i=1}^{n}(S_i - \bar{S})^2 \sum_{i=1}^{n}(R_i - \bar{R})^2\right)^{1/2}} \quad (4)$$

where S are the observations (buoy or satellite measurements), R are the reanalysis values, the overbars indicate mean values through time and n denotes the number of data pairs. Error metrics were calculated for co-located pairs of buoy and reanalysis data points. Since the main focus in the present study is on extreme events, the same metrics were also calculated for the values above the 95% and 99% percentiles. Finally, the ratio between the CFSR quantile divided by the buoy quantile were also computed, for the same levels of 95% and 99%, which means the inverse of the Cumulative Distribution Function (CDF) of the reanalysis related to the buoy. Whenever this ratio is above 1.0, the wind speed of CFSR is greater than the buoy and when it is below 1.0 the wind speed of the buoy is greater than CFSR. This ratio can be useful to visualize any possible overestimation or underestimation of CFSR for different intensity levels.

Table 1. CFSR winds compared to three offshore buoys in Brazil. Error metrics are also applied to values above the 95% and 99% percentile levels (p95 and p99 labels). Metrics are correlation coefficient (CC), mean error (ME), root mean square error (RMSE), and scatter index (SI).

buoy	CC	ME	RMSE	SI
1	0.85	-0.08	1.47	0.45
2	0.85	1.17	1.76	0.23
5	0.67	1.93	2.22	0.30

buoy	ME.p95	RMSE.p95	Si.p95	ME.p99	RMSE.p99	Si.p99	$\frac{QU_{p95}^{CFSR}}{QU_{p95}^{buoy}}$	$\frac{QU_{p99}^{CFSR}}{QU_{p99}^{buoy}}$
1	0.51	2.58	0.15	0.66	1.67	0.08	0.95	0.96
2	1.14	3.36	0.18	1.06	2.09	0.10	0.91	0.94
5	-0.48	0.99	0.08	-0.88	1.60	0.12	0.82	0.96

Table 1 presents bulk results, including upper percentiles (more severe sea states). Before making assertions on the quality of CFSR winds relative to available buoy data, two limitations must be considered. First, the short measurements duration at buoys 2 and 5 cast doubts on the reliability and statistical significance of their data. Second, even considering the longer buoy 1 dataset, measured 95% and 99% percentiles had most intense winds at 14 and 17 m/s, respectively, which also cast doubts to their being representative of “true” extreme conditions. Therefore, the term “extreme” referring to upper percentiles in Table indicate wind intensities above 14 m/s – which for several other locations with severe climate would not be at all extreme.

Table shows a relatively good agreement between CFSR and buoy data, with CC around 0.8 and small ME and RMSE. On the other hand, the SI is reasonably high, which indicates that ME and RMSE are low partially due to the small intensities and not necessarily because of the good accuracy of CFSR. For general conditions (upper lines of the table) at buoy 1, CFSR slightly overestimates wind intensities, whereas at buoys 2 and 5, CFSR underestimates them. Moving to the upper percentile of 95%, the ME increases at buoy 1 and CFSR starts to underestimate the events. ME values increase even more at the percentile of 99%. The ME and RMSE become higher under extreme conditions, whereas SI are reduced. Therefore, the reanalysis does not necessarily deteriorate moving to extreme events; the precision showed small changes and the accuracy indicated an increasing reanalysis underestimation at buoy 1 with intensity.

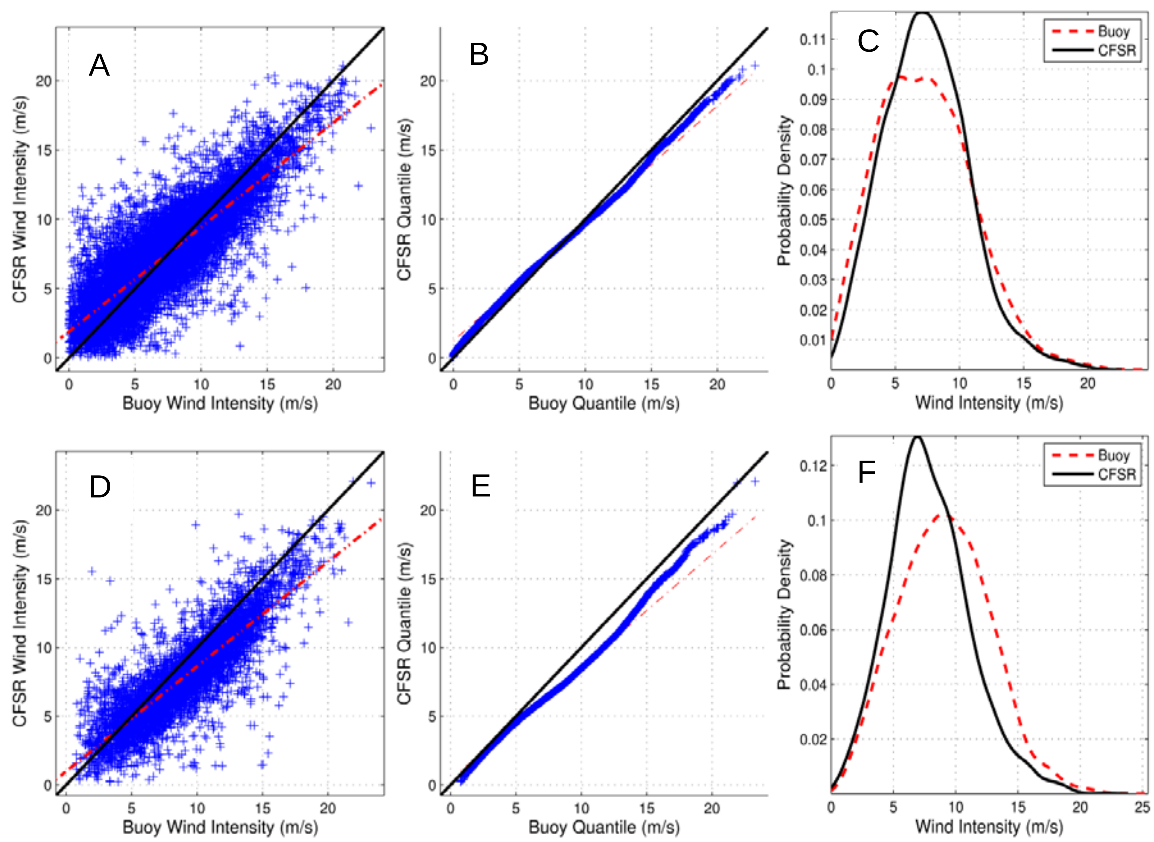

Figure 4 – Scatter plot (on the left; A, D), QQ-Plots (center; B, E) and Probability Density Function (on the right; C, F) comparing the CFSR wind intensities (y-axis) with buoy wind intensities (x-axis). The first line (A, B and C) represents buoy 1 while second line (D, E and F) represents buoy 2.

An alternative way to analyze the performance of the reanalysis with the intensity is by looking at the scatter plots, QQ-plots and probability distributions, shown in Figure 4. The scatter plots indicate a large spread of co-located CFSR and buoy data. The QQ-plots indicate a good representation of CFSR winds for wind intensities up to 10 m/s. From that point, CFSR moderately, but consistently underestimates higher wind speeds. The probability density functions show that the shape of the functions diverges, mainly in terms of kurtosis, which impacts long-term distributions fit and extrapolations.

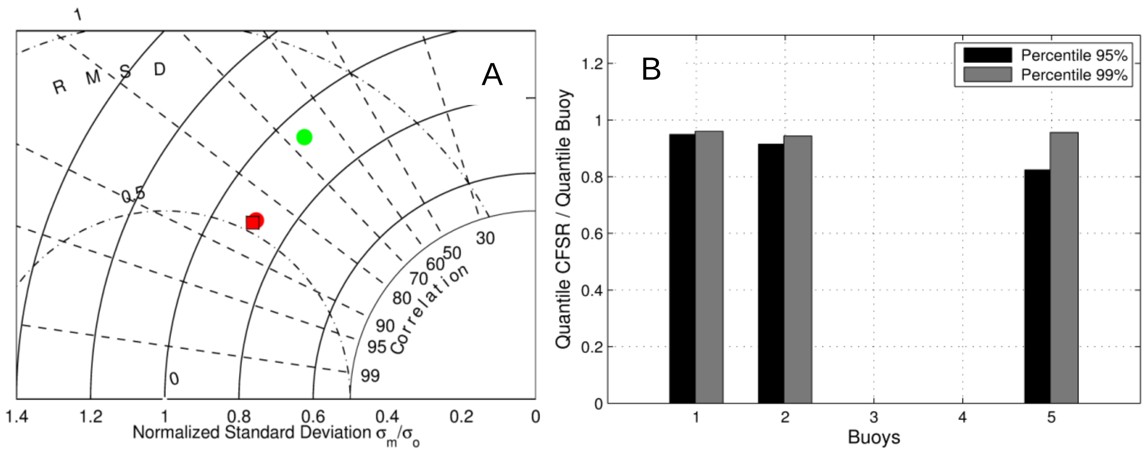

Figure 5 – Summary of results comparing CFSR wind intensities with buoy data. Taylor Diagram (BLT) on the left; the red square and red circle dots are buoys 1 and 2, at Rio Grande do Sul, while the green circle is buoy 5, at Espirito Santo. Quantile ratios for 95% and 99% levels on the right.

Validation statistics are further summarized in Figure 5, showing an inverted Taylor diagram (Taylor, 2001), the so-called BLT diagram adapted by Alves et al. (2014). The correlation coefficient, normalized standard deviation and the root mean square difference for each buoy are presented in the same plot. Buoys 1 and 2 are overlapped on the diagram, with very similar results, while buoy 5 has very different metrics with large differences between CFSR and buoy. Three reasons might create these differences in buoy 5: further north position, with a different wave climate; the short duration of the measurements (which makes direct comparisons with buoys 1 and 2 inappropriate); and the buoy construction and type, representing an experimental instrument with lower reliability. Figure 5, on the right, shows the extreme quantile ratios, confirming the small underestimation of CFSR that does not increase from 95% to 99% percentile – in fact there is a small reduction of the underestimation at the 99% level.

Although the CFSR evaluation using buoy data is a relevant first step to qualify the reanalysis, the available buoy dataset is not sufficient for a proper statistical analysis, regarding both temporal and spatial coverage. In the next section, this limitation is attenuated via the use of satellite data, which makes possible a better evaluation of the cyclonic winds that generate the most extreme waves during the period 2002 to 2009.

4. Evaluation of CFSR relative to scatterometer winds

In this section surface wind speeds from the CFSR are compared to measurements made by QuikSCAT during severe weather events associated with extreme significant wave heights (Hs) in the western South Atlantic. Comparisons are made using a grid with resolution of 0.25° X 0.25° and preserve the time of QuikSCAT tracks, whereby CFSR data are interpolated in space and time to match measurements. This approach allows building pairs of co-located CFSR and QuikSCAT data for any given QuikSCAT track. Given the goal of the present study to improve CFSR surface winds associated with extreme wave events in Brazil, wave measurements were used to select the periods when extreme wave heights occurred. For this purpose, extreme conditions were elected whenever wave heights exceeded the 99th percentile. Using this criterion, a total of 47 events were identified, and time series of paired CFSR and QuikSCAT data were generated accordingly, including 72h lead up before the observed time of maximum wave height.

The use of QuikSCAT data under extreme wind conditions above 20 m/s might be considered questionable, since the scatterometer has increasing uncertainties for high intensity storms with heavy clouds (Freilich and Vanhoff, 2006; Quilfen et al., 2007). However, Quilfen et al. (2007), after performing a complete evaluation of QuikSCAT data, found that wind vector retrieval under extreme condition is feasible. Besides, the conditions considered “extremes” in extra-tropical cyclones in the southwest Atlantic are much less intense than those associated with tropical cyclones in the North Hemisphere.

Table 2 - The nine most extreme events of Hs measured by Brazilian buoys in deep waters until 2010. Hs (meters). Tp (seconds). Dp (degrees).

Date	Hs (m)	Tp (s)	Dp (°)
28/06/2006	6.11	11.8	221.5
30/07/2006	7.05	13.7	209.7
29/07/2007	6.13	13.8	208.0
25/09/2007	6.41	12.6	213.9
16/06/2008	7.61	13.4	207.6
11/04/2009	6.20	14.9	200.3
29/05/2009	6.01	14.0	193.6
21/08/2009	6.05	10.9	155.5
13/12/2009	6.67	12.1	145.4

Looking carefully at each event individually is critically important but very time consuming when 47 cases are involved. Therefore, a bulk analysis is presented. For the purpose of illustrating the more detailed analysis carried out, nine most severe events were selected from the sample of 47, as indicated in Table . In agreement with studies reviewed in our introductory section, the nine selected extreme events are associated with peak wave periods from 11 to 15 seconds, and directions from southeast to southwest. Most part of the events occurred during winter and fall - only one event was registered during summer. Below, an analysis of each of the selected nine events is provided, focusing on the general synoptic features, as well as the quality of CFSR data relative to QuikSCAT.

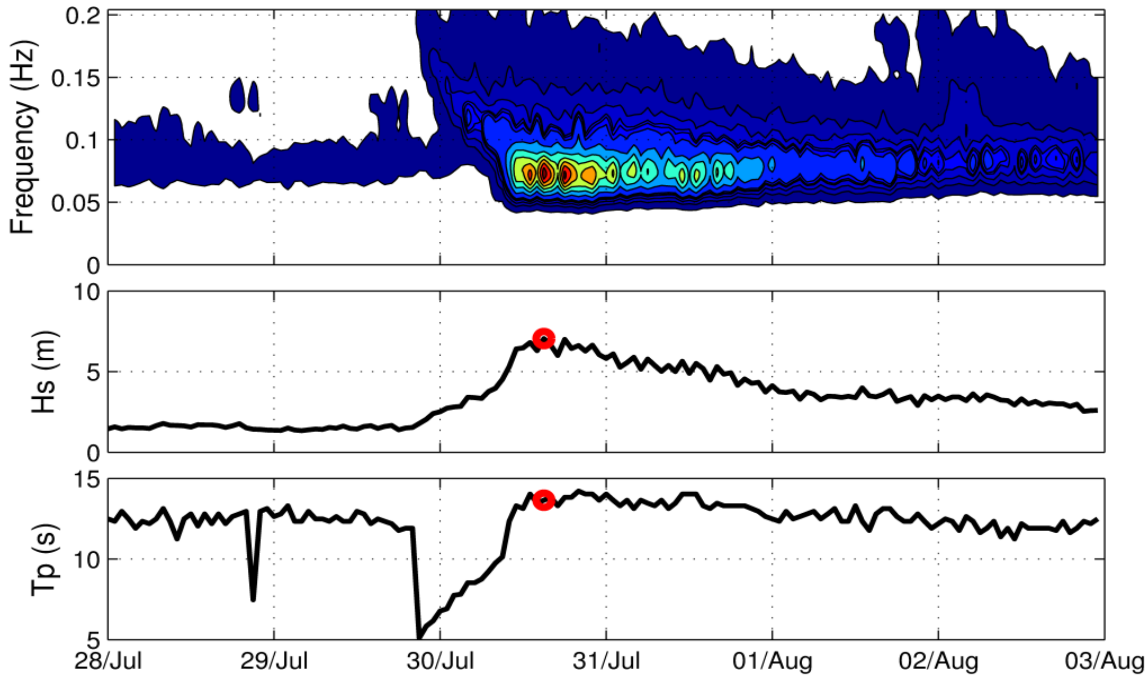

Figure 6 – Evolution of the most extreme event of significant wave height, in July of 2006. The top plot shows the time sequence of power spectra. The significant wave height (Hs) and spectral peak period (Tp) are plotted bellow it. The red dot indicates the instant of maximum wave height.

For the selected period, the most extreme Hs event occurred on July 30 2006. Figure 6 shows the time evolution of 1D spectra, alongside time series of Hs and peak period (Tp). It is possible to see the fast growth of waves and periods, starting during the last hours of July 29 and with the peak in the afternoon of July 30. Synoptic conditions shown in Figure 7 reveal that a cold front with strong southerly winds hit the southeast coast of Brazil before the maximum of wave heights, as indicated in the spectral evolution of Figure 6. The fetch is associated with a cyclone generated around the mouth of Rio de La Plata, between Uruguay and Argentina, at around 38°S. The cyclone quickly propagated towards east, then southeast, creating a very large fetch that dominated the left part of the cyclone. As seen in Figure 7, winds initially generated waves within a relatively short-to-medium fetch with intense winds of 25 m/s on the July 29. As the cyclone evolved, a much larger fetch developed on July 30, with lighter winds of 15 m/s.

Figure 7 panels D, E and F illustrate the difference between QuikSCAT and CFSR surface winds. Although CFSR reanalysis assimilated QuikSCAT from 2001 to 2009, the evolution of the cyclone shows that CFSR consistently underestimates measurements within the cyclone, especially at the left part of the low pressure system associated with southerly winds, indicating the weight of surface winds assimilation was not significant. Differences are around 5 m/s in a relatively small area with strong winds, and from 2 to 3 m/s over the larger fetch. This represents an underestimation of 10% to 25%, in areas where QuikSCAT is more intense than CFSR.

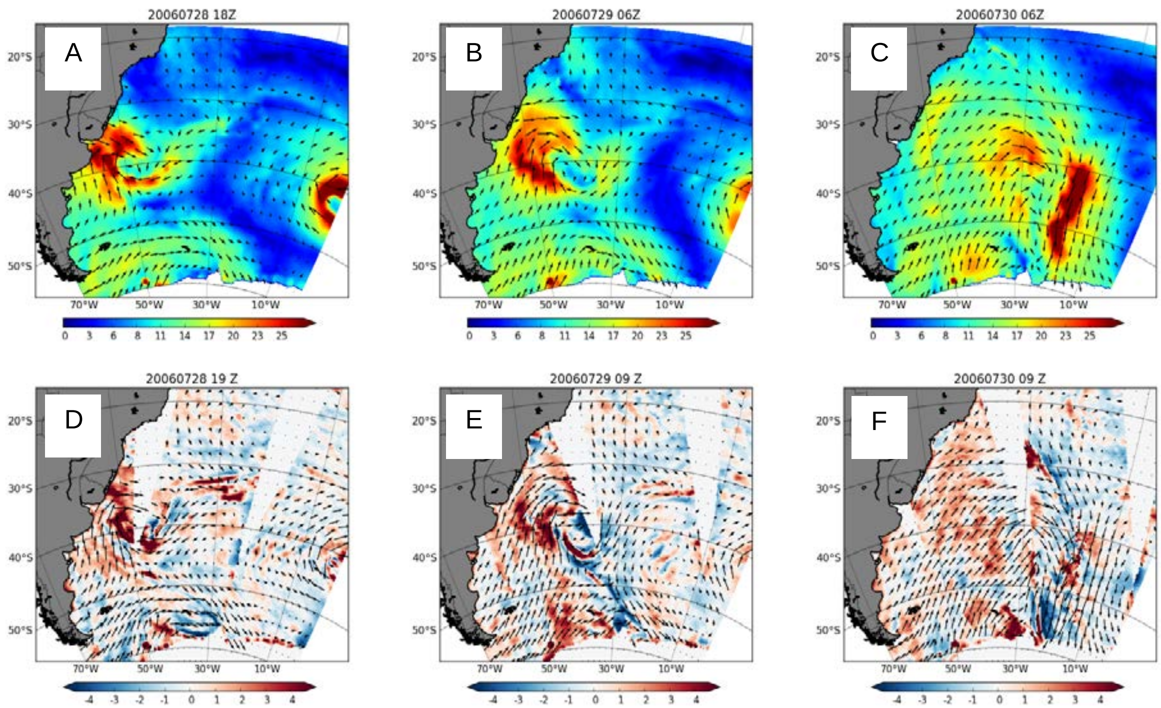

Figure 7 - Surface winds in the South Atlantic Ocean, synoptic evolution that generated the most extreme waves recorded in Brazil, in July of 2006. First line (A, B and C): SeaWinds 10-meter winds (m/s). Second line (D, E and F): QuikSCAT winds minus CFSR winds (m/s).

Other extreme events from Table 2 were also analyzed in the same way. In all cases, cyclogenesis, fetch positioning and evolution were very similar. CFSR underestimation was present in all the extreme events, as in Figure 7, with differences from 2 to 5 m/s in regions of higher wind speed. It is important to note that areas with the largest CFSR underestimation were found to be very close to the center of the cyclone. Unfortunately, in all selected events cyclonic winds did not affect directly any of the available buoys, so the worst cases of misrepresentation of CFSR winds could not be measured and presented in Table and Figure 4 and Figure 5 – which increases the importance of an independent evaluation using satellite data.

Considering that the atmospheric conditions in the South Atlantic Ocean associated with the most extreme Hs events are reasonably similar, and the analysis and inclusion of many figures would make this paper unnecessary long, it was decided to present a composition of all extreme events in terms of the average surface winds before the peak of the wave measurement. We call these images "composites", and they indicate regions containing the most differences between CFSR and QuikSCAT, as well as the time evolution of the CFSR underestimation areas.

4.1. Cyclone Identification

Prior to building composites, a cyclone tracker based on Murray and Simmonds (1991), Sugahara (2000), Reboita (2008) and Kurihara et al (1993) was implemented to identify the center of cyclones and to calculate maximum and average parameters of atmospheric variables within storms. The method consists of identifying all cyclone positions in the domain with latitudes 87°S to 5°S and longitudes 82°W to 22E°, from 2002 until 2009, using the mean sea level pressure and zonal and meridional surface wind fields. In addition to Murray and Simmonds (1991), the algorithm constructed is also based on Gan and Rao (1991), Sugahara (2000), Reboita (2008), Reboita et al. (2009) and Campos (2009).

First, a window is defined with 24° X 24° of latitude/longitude encapsulating the input fields, where a search is performed for local minimum values of vorticity (negative in the southern hemisphere) and pressure, both at the surface. This initial identification forms a group of candidate storms that then have to pass criteria such as maximum vorticity, maximum mean sea level pressure and minimum wind speed. After many sensitivity tests, the mean sea level pressure was set as secondary variable and the vorticity and pressure gradient became crucial to identify the stronger cyclones.

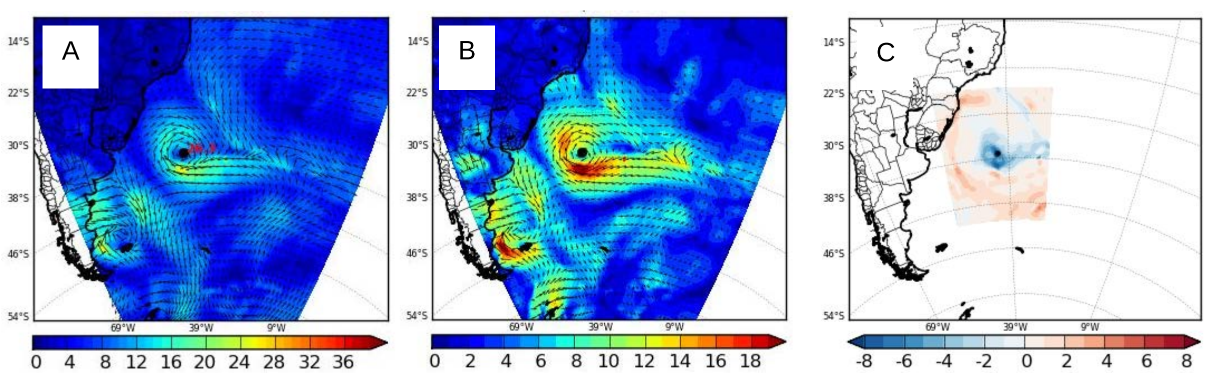

Figure 8 - Cyclone event at 12Z on 27/12/2006. Left figure (A): Original CFSR 10-meter wind field. Center (B): Disturbance CFSR field, removing low frequency atmospheric waves (Kurihara et al., 1993). Right (C): Vorticity field highlighting the center of the cyclone and the cyclonic circulation.

Initial results indicated that South Atlantic cyclone vary significantly in terms of size, intensities and evolution, confirming previous studies by Reboita (2008) and Reboita et al. (2009). Therefore, by using the same restriction values for the cyclone identification in the whole domain, some areas were benefited and others became too restrictive. For instance, cyclones in southern latitudes were easily detected while less intense cyclones close to Brazil were missed. The correlation between cyclone intensity and cyclonic variables were calculated, which pointed a strong relation between intensity and latitude. Hence, instead of using the same criteria for the entire domain, new criteria were re-defined as a function of latitude. This allowed a better identification of cyclones closer to the coast and within subtropical latitudes, which are essential for the present study.

Subsequent results confirmed that the algorithm was working correctly. However, a few small cyclones were still missing, including the hurricane-like cyclone Catarina (Silva Dias et al., 2004; Pezza and Simmonds, 2006; Pereira Filho and Lima, 2006), one the most extreme storm events ever recorded near the southern Brazilian coast. It was soon found that the reason for the non-detection was not the cyclone tracking algorithm, but the input CFSR fields misrepresenting some extreme events with small dimensions, quick evolution and strong winds confined to a small area. This was overcome by performing a second round of cyclone identifications using an alternative source: blended surface winds measured by satellites, available from the SeaWinds blended database. Due to unavailability of mean sea level pressure, identification was made using surface winds and vorticity only. In order to enhance vortices and events with strong vorticity, the method of Kurihara et al. (1993) was applied, which facilitated the identification, as illustrated in Figure 8. Test runs for 2006 revealed that 8.45% of the cyclones in that year were successfully identified in the SeaWinds database but not in the CFSR. On the other hand, 12.67% were identified using CFSR and not in SeaWinds, whereas 3.07% of the cyclones identified in the latter had incorrect calculated positions, probably due to the lack of additional variables such as the mean sea level pressure.

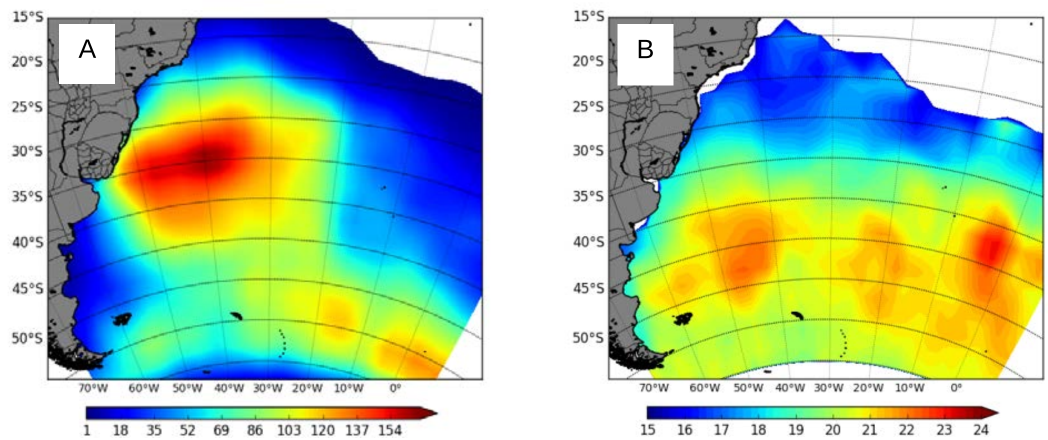

Figure 9 - Occurrence of individual cyclones identified (on the left) and average maximum wind speed (m/s), at 10-meters level, within the cyclones (on the right).

Final cyclone occurrences and positions for the whole period were built as a composition of the two identification processes, with CFSR and SeaWind combined, prioritizing CFSR identification. A database was created including latitudes, longitudes, dates, minimum, maximum and mean wind intensities, vorticities and pressures for each cyclone. Figure 9 presents a spatial view of results. On the left, the occurrences of cyclones show a high density at 35°S, close to Uruguai and Rio Grande do Sul. Although the cyclone identification is larger around this latitude, the greatest intensities are found below 40°S. Events at north of 35°S present much lower values of wind speed than those at extra-tropical latitudes. Campos et al. (2012) discuss this balance between positioning and intensity associated with the severity of extreme events in Brazil.

4.2. Composites of extreme winds

The cyclone identification was applied to the 47 extreme events selected on the basis of buoy data. Table shows the average position of associated cyclones, average wind speed, average mean sea level pressure and maximum wind speed. The number of selected events is related to the top 1% independent events measured by the wave buoys - in all cases they were generated by cyclones. The first column of Table shows 72-hour periods before the peak of the extreme event as measured by the buoy. In most cases, cyclogenesis occurred 48 hours before the peak waves. However, some cases had a longer wave build-up process, so a 72-h period was added.

Table 3 - Average position and variables of the cyclones associated with the 47 extreme events of wave heights measured by metocean buoys in Brazil. The average is calculated for each instant before the maximum wave measured, from 00 hours to 72 hours before. MSLP: Mean Sea Level Pressure (hPa). U_{10m}: 10-meters wind intensity.

Lead Time	Lat	Lon	MSLP (hPa)	$\overline{U_{10m}}$	U_{10m}^{max}
00	-39.03	-38.47	961.9	12.10	28.52
06	-39.53	-37.09	958.6	12.02	27.70
12	-39.46	-38.44	961.8	11.83	31.36
24	-40.80	-38.05	962.8	12.53	29.29
48	-41.22	-41.62	949.4	13.81	30.04
72	-41.32	-41.28	964.6	11.94	31.30

In terms of cyclogenesis and position, the latitude changes little through the cyclone evolution prior to the extreme wave events in Brazil, around 40°S, whereas the longitudinal track moves towards east. The mean sea level pressure (MSLP) has the lowest values at 48 h and 6 h, while the average wind speed has highest values 48 h before the peak of the wave measurements. Maximum winds within cyclones are most intense 12 h before peak measured waves. Both wind speed and mean sea level pressure show lower intensity at the time of the peak of the waves.

Figure 10 summarizes the error of composites of CFSR surface wind speeds relative to measurements, for up to three days before peak wave occurrence, considering the top 1% of extreme wave events measured by available buoys. The overall highest values seen in Figure 8 are damped, as a consequence of spatial averaging applied to maximum cyclone winds that are restricted to small areas, leading to a mismatch in positioning from one cyclone to another. Regardless, the spatial distribution clearly shows some important characteristics governing the occurrence of wave extremes. Average wind intensity and direction confirm the well-known persistence of southwesterly winds in southern Brazil, Uruguay and northeast Argentina. Strongest winds are found again 48 h before wave maxima are observed. Agreeing with Figure 8, the intensity of surface winds drop around the time of maximum wave height occurrence.

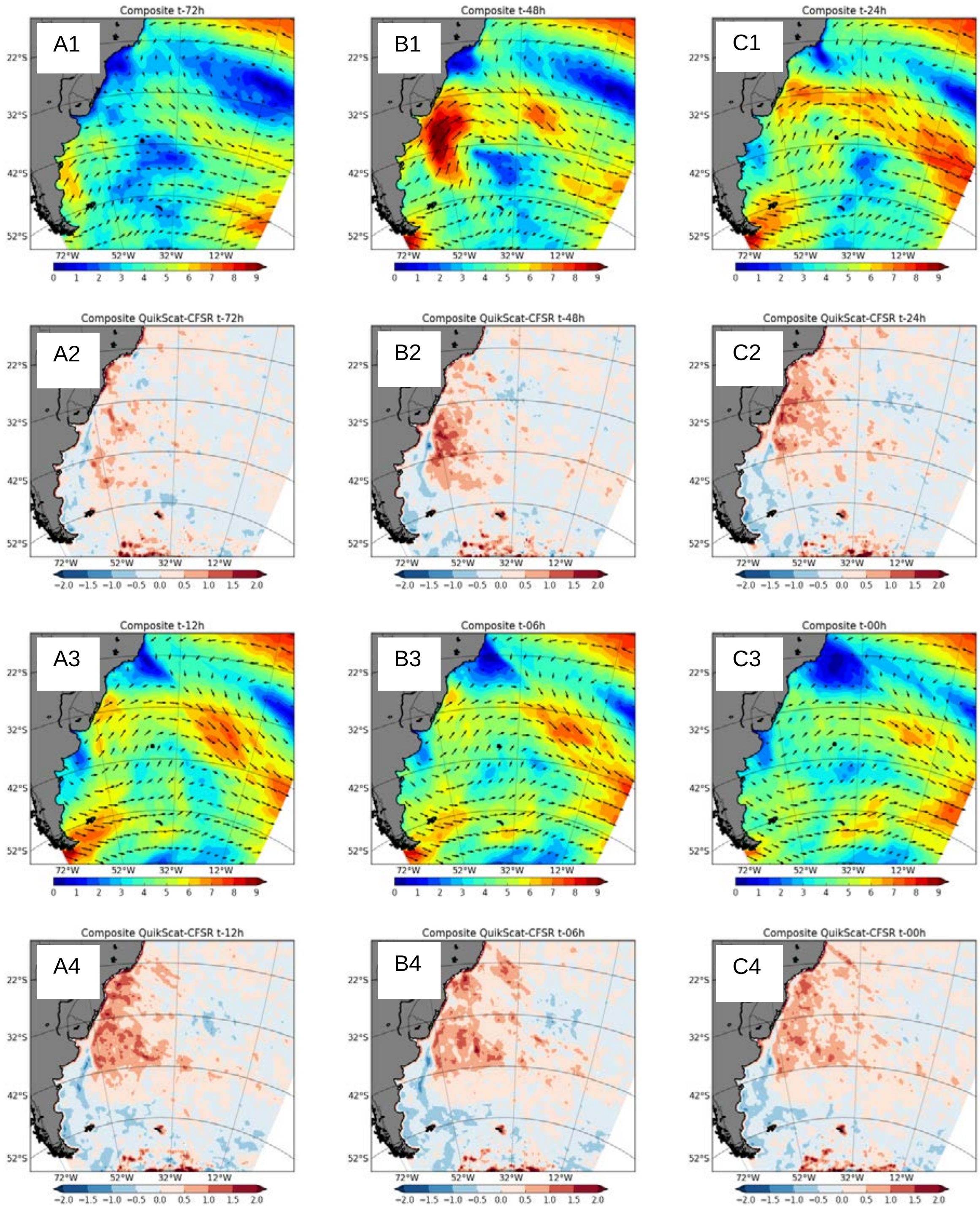

Figure 10 - Composites of wind intensity (first and third lines, m/s) and wind intensity difference of QuikSCAT minus CFSR (second and fourth lines, m/s). Average at each hour before the maximum wave measured in Brazil, from 00 hours to 72 hours before.

Rows 2 and 4 in Figure 10 present the differences in wind intensity QuikSCAT minus CFSR. Maps confirm that CFSR generally underestimates intensities in the area of maximum winds, mainly associated with southerly directions. The average underestimation varies from 1 m/s to 2 m/s, especially in the western part of the Atlantic Ocean, close to the coasts of Argentina, Uruguay and Brazil. The evolution in time indicates a displacement of the CFSR underestimation area, following cold fronts coupled with the tracked cyclones. Underestimation becomes more significant 48 h prior to maximum waves, mostly at southern latitudes. Around 24 h prior to maximum waves, the largest underestimation (red shaded areas) shifts northward, nearing southeastern Brazil and 20°S. In the 12 h lead to maximum measured waves, the underestimation persists with more or less the same spatial extent, having a small spread towards eastern longitudes. Surface winds are the most important variable for the numerical wave forecasts. Figure 10 maps regions that must be carefully investigated as potential sources of largest inaccuracies in winds used for simulating extreme waves in the south and southeast of Brazil.

5. Improved Winds for Extreme Wave Simulations

It was shown above that the CFSR surface winds are generally skillful for ambient conditions, but consistently underestimate the highest observed wind percentiles, when both buoys and, particularly, scatterometer data are considered. When compared to QuikSCAT, CFSR showed large errors around 5 m/s within the cyclones with wind intensities up to 35 m/s. These inaccuracies at stronger wind speeds are crucial for extreme wave simulation. Therefore, an adjustment method was investigated to improve CFSR higher-percentile winds in the South Atlantic Ocean.

In view of the availability of measurements with different characteristics used for the CFSR evaluation, we performed a series of alternative calibration approaches as follows. First, a very simple univariate linear regression model is applied using buoy measurements – a quick and widely-used solution in the private consultancy industry. Thereafter, more complex methods using several satellite measurements, merged with the CFSR reanalysis within the area of influence of cyclones are applied. A discussion of results is then presented. The ultimate objective of the calibration performed below is the generation of a consistent, high-quality surface wind database, optimally adjusted to force a wave model. Campos et al. (2017) shows that this provides a wind forcing database that allows both ambient and extreme waves to be skillfully simulated.

5.1. Linear regression model

The use of a linear regression model is a common approach to calibrate wind intensity and wave height in several applications, using observations or numerical prediction models. A classic paper on the topic is Tolman (1998), where several correction approaches using linear regression are applied to atmospheric model wind speeds used for operational forecasting of wind wave at the US National Weather Service. An extension of that method, for calibrating surface winds for use in wave hindcasts for the South Atlantic Ocean is provided in Alves et al. (2009). In the latter, which is relevant in the context of the present study, the authors found the following linear relationship for surface wind calibration in the region:

$$U_{corr} = 1.17\,0.\,U_{mod} + 1.05 \quad (5)$$

where *Ucorr* is the corrected wind speed, and *Umod* is the input wind speed from the atmospheric model dataset.

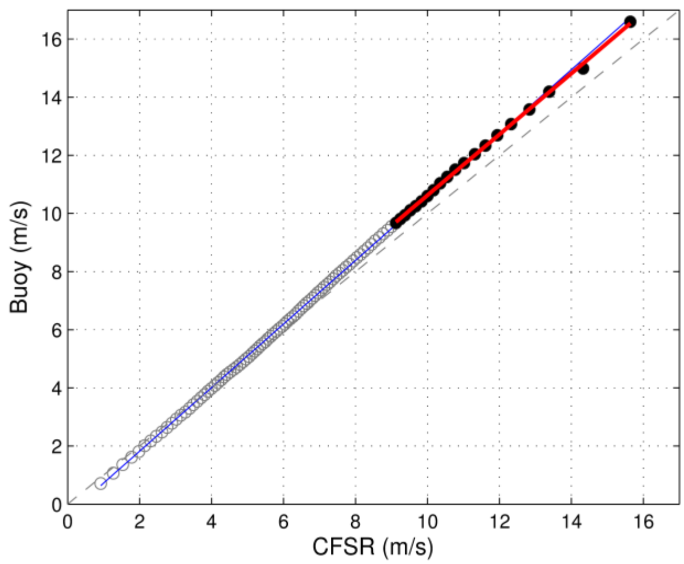

Figure 11 - Buoy quantiles versus CFSR quantiles for 10-meters wind intensity. Grey line shows a linear regression fit considering all quantiles while the red line shows the fit to quantiles above the percentile of 80% (approximately 10 m/s).

For wave data, an example of linear regression calibration is found in Caires & Sterl (2005), who calculated global extreme values of wave heights using the ECMWF reanalysis ERA-40 (Uppala et al., 2005). They verified a large underestimation of extremes, confirmed more recently by Campos and Guedes Soares (2016a), whereby the proposed solution was to calibrate the ERA-40 wave heights using buoy data, by applying a linear regression model, and verifying results against Topex/Poseidon data. After calibration, a significant improvement was found in the upper percentiles, which reflected in more reliable extrapolated extreme values. Their proposed calibration was:

$$H_s^{Buoy} = 0.52 + 1.30.\,H_s^{ERA-40} \quad (6)$$

We applied a similar approach used by Tolman (1998) and Alves et al. (2009). Pairs of wind data, converted to 10 m height where needed using the LKB method, were built from CFSR and buoys. These were used to calculate quantiles ranging from 1% to 100%, stored in two arrays of 100 points. Results were plotted as illustrated in Figure 11 (black dots). Two linear regression fits were calculated: one for the whole set of quantiles (grey line), and another for the values above the 80th percentile (red line), approximately above 10 m/s. Equations 7 and 8 are the resulting linear regression models adjusted to the bulk percentiles, and to the upper percentiles only, respectively.

$$U_{10m}^{corr} = (1.094 * U_{10m}^{CFSR}) - 0.370 \tag{7}$$

$$U_{10m}^{corr} = (1.049 * U_{10m}^{CFSR}) - 0.140 \tag{8}$$

A first candidate wind database for application to simulation of wave extremes (e.g., Campos et al., 2017), was built applying equation (8) to the CFSR winds in the South Atlantic Ocean (CFSR.LR). Only the wind intensity is calibrated, the direction remains the same. Changes obtained with this approach represent an increase of 5% to 6% of the CFSR wind intensity within more severe storm systems observed in the South Atlantic.

5.2. Cyclonic Wind Replacement and Blending

The evaluation of CFSR surface winds indicates that it severely underestimates upper-percentile winds within cyclones in the South Atlantic. In some cases, the CFSR data misses completely events that may be associated with some of the most extreme cases (e.g., the cyclone Catarina). An original method devised as part of the present study is proposed where the perceived deficiencies of the CFSR cyclonic winds are remedied, whereby "defective" wind fields are replaced with data measured by satellites, and the consistency of overall fields ensured by a blending algorithm.

Replacement and blending are performed following the center of cyclones, with centers identified by the cyclone tracking previously explained. The basis of the proposed approach follows three general steps. First, cyclones are identified following the technique proposed in Murray and Simmonds (1991), described in section 3.1. Second, cyclonic wind fields are isolated from the background/ambient wind signal following the approach of Kurihara et al. (1993). Finally, new cyclonic winds are added to the background field, following loosely the approach pioneered in wave modeling by Chao et al. (2005).

a. Extracting CFSR Cyclones

After cyclones in the CFSR database are identified, as described in section 3.1, the key step of the process is to separate cyclonic winds from the background, ambient fields, and extract them for replacement. This is done following the method suggested by Kurihara et al. (1993). Separating these two wind-field types is crucial for the development of a sound, calibrated database. Kurihara et al. (1993) use iterative filters to remove high frequency disturbances from the large-scale wind fields so that a smooth environmental field is produced. The latter is retained, and provides the ambient component of the new surface wind field database. An example of the procedure is given in Figure 12, panels A, B and C.

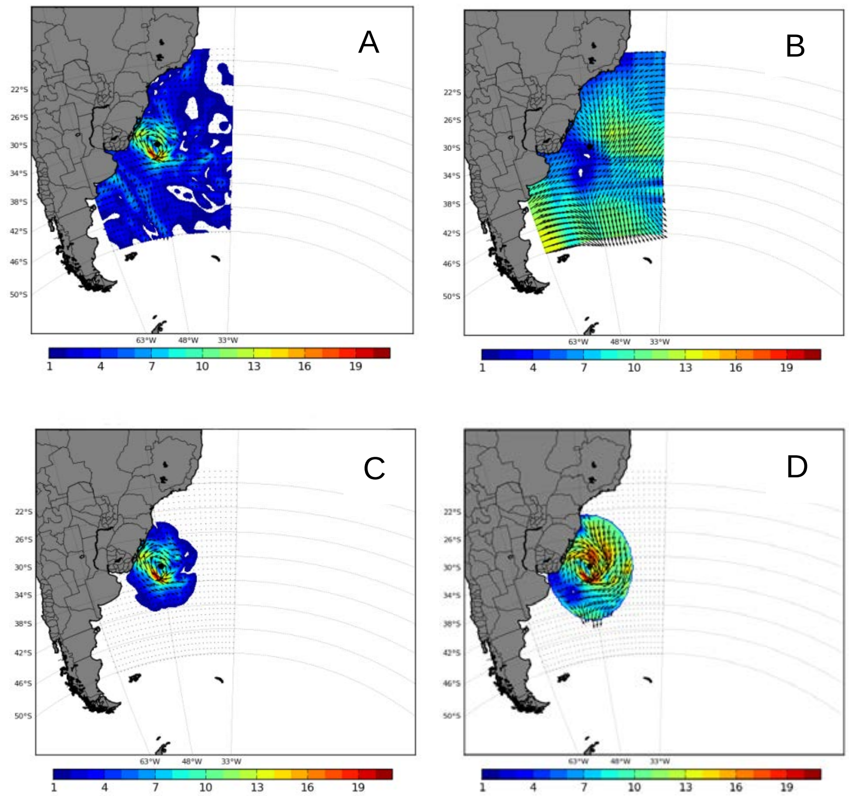

Figure 12 - Example of application of the method proposed by Kurihara et al. (1993) for a cyclone at 12Z on 24/03/2006. A: Disturbance wind field. B: Environmental field without the cyclone. C: Analyzed vortex with the cyclone isolated. D: Original cyclone selected within a specific radius.

b. Cyclonic wind specification

The original idea for cyclonic surface wind specification was to use directly QuikSCAT measurements to replace removed perturbations from the CFSR data. Inspection of the data during selected severe cyclonic events, however, revealed too many spatial and/or temporal gaps in the available data, in a way that would affect our ability to reconstruct a consistent time series of cyclonic wind fields throughout the lifetime of many events. Insight on how severely QuikSCAT under-samples small-scale, rapidly changing systems is provided in Figure 3A. Clearly seen are spatial gaps of hundreds of kilometers that could easily hide an entire small-scale system. Also, time lags of several days and little overlap between swaths are noticed.

A surrogate measurement database was sought that could be used in combination with QuikSCAT, allowing the reconstruction of surface winds from each cyclonic event in a more reliable way. The SeaWinds database, described previously, was selected for that purpose. This choice allowed us to also build two additional blended products, one using SeaWinds only, and a second using SeaWinds in conjunction with QuikSCAT in a way that maximized the use of the latter. Since QuikSCAT is one of the remotely-sensed data sources used in SeaWinds, the combination was largely consistent, requiring a minimum of adjustments in the blending process.

SeaWinds is a 6-hourly satellite database, which needed to be interpolated onto the 1-hourly sampling rate from the CFSR database. Tolman & Alves (2005) have shown that direct application of a traditional bi-linear interpolation deteriorates the structure of small cyclones containing strong winds with fast propagation, the so-called “German-salsa” effect, which can lead to wave fields with negative biases of the order of 10%-20%. The latter results from an artificial aliasing due to the linear interpolation which does not account for the spatial displacement of the storm centers that occurs between two consecutive 6 h intervals. This limitation is crucial in the present paper, due to the concern about the representation of the extreme winds. Therefore, we here follow the suggestion of Tolman & Alves (2005) to separate the cyclonic and background winds from the SeaWinds database, following again the approach of Kurihara et al (1993), and to perform separately background and storm-centered interpolation between consecutive SeaWinds time slices, providing hourly wind fields, which are then recombined onto a consistent hourly SeaWinds database (henceforth SW1h).

Figure 12 exemplifies the process for a cyclone generated in the southern coast of Brazil, in March 2016. This example illustrates also an adaptation of the Kurihara et al. (1993) method that was needed for its application to extra-tropical storms in the South Atlantic. Originally, that method dealt with tropical cyclones in the North Atlantic, which present strong distinctions relative to extra-tropical systems. Hurricanes usually have a symmetric and circular shape with clear boundaries. Extra-tropical cyclones are always associated with large troughs and cold fronts with large fetches, where the boundaries are less clear. In the southern hemisphere, fetches with meridional winds are mainly located on the left of the troughs.

These differences led to occasional problems during the extraction of the extra-tropical cyclones following strictly Kurihara et al. (1993), namely, the exclusion of the vortex created large gaps in the environmental field that, when interpolated in time, would grow into “trenches” that could not be completely masked by re-insertion of the interpolated vortex. This problem was solved by applying the Kurihara et al. (1993) method only for the construction of the environmental field, as shown in panel Figure 12B. The extracted cyclonic field was then simply taken without any filtering (no removal of the background signal), and interpolated to hourly slices retaining the original wind field within the area inside the extraction radius, as shown in Figure 12D. Resulting hourly cyclonic fields were finally completely inserted on the hourly environmental field, replacing the winds within the cyclone limits. A smoothing function using simple linear combination is applied at boundaries to ensure continuity between background and cyclonic fields.

c. Resulting blended satellite-based CFSR-enhanced database

The blending of CFSR ambient fields with satellite-based cyclonic wind fields generated two distinct classes of surface wind databases. The latter are used in an extreme wave analysis study reported in Campos et al. (2017). The two classes of hybrid model-satellite wind databases differ only in terms of the CFSR ambient winds, which in the first class has no calibration applied to background winds, while in the second set the linear regression is used to calibrate the CFSR ambient winds. Both classes of corrected winds intake satellite data of SW1h and QuikSCAT within cyclones using the same methodology. In this section we present relevant examples of the resulting blended winds during severe cyclonic events with different characteristics relevant to generating wave extremes.

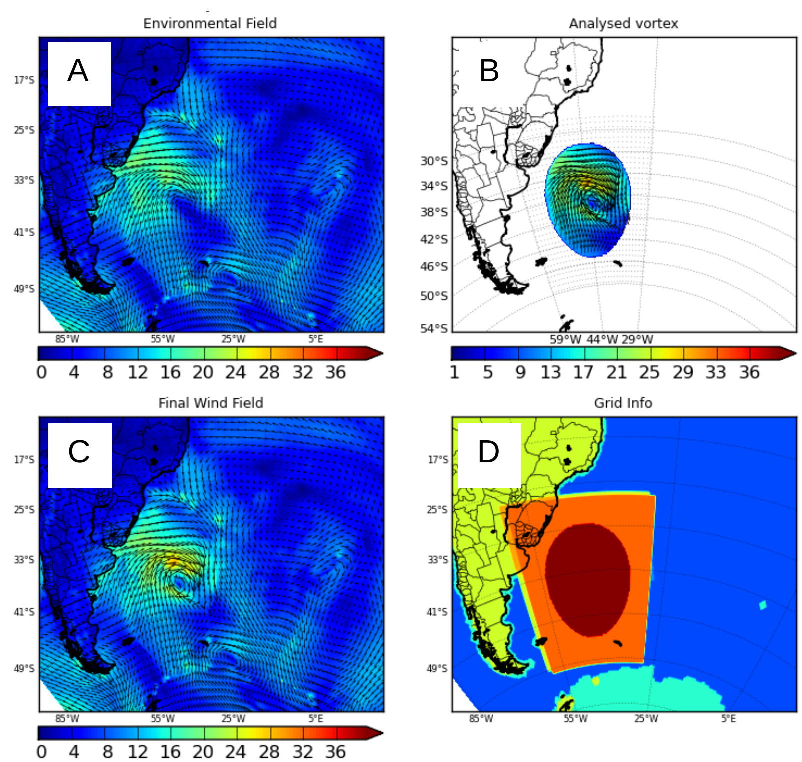

Figure 13 - Example of centered interpolation of SeaWinds (m/s) for 08Z on 17/06/2008, the cyclone event that generate the most extreme event measured in southeastern Brazil (Hs=7.6 meters). Figure D: in blue the original wind without modification, in cyan the excluded points associated with ice or coastal grid points, in dark red the area where the cyclone was centered-interpolated and inserted, in orange the transitioning area.

Blended fields associated with an extreme wave event on 17 June 2008 are shown in Figure 13, when the depicted cyclone generated wave height in excess of 7.6 m offshore southeastern Brazil. Figure 13A presents the environmental field with only low-frequency atmospheric waves retained, where a large trough is observed. The analyzed vortex is shown in Figure 13B, preserving the full SW1h surface wind data. The blended wind field is shown in Figure 13C, in which the cyclonic winds have been grafted onto the environmental field with a smoothing function applied to the boundaries between them. Figure 13D illustrates the stencils used in the blending process: the dark red stencil is the area where the cyclone was inserted, and the orange stencil marks represents the transitioning area where smoothing is applied, consisting of a running window following the center of the cyclone over time.

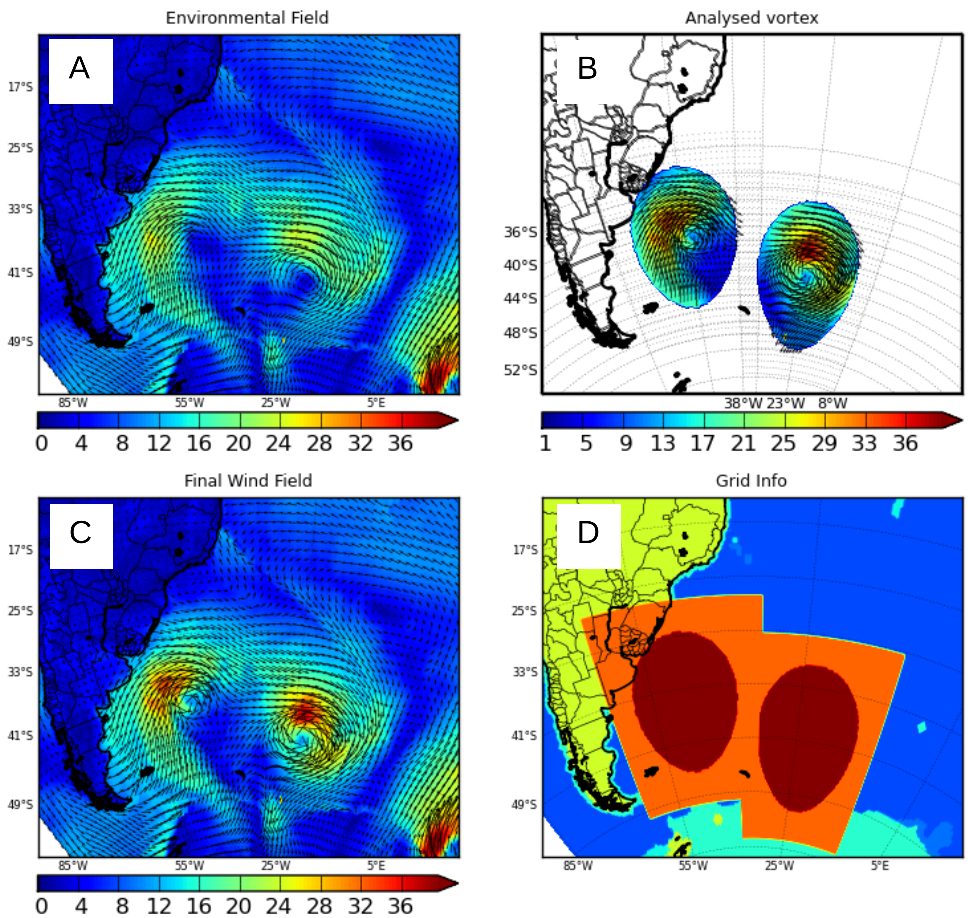

Figure 14 - Example of SeaWinds centered interpolation with two cyclones at 05Z on 27/07/2007.

Figure 14 presents other example of centered interpolation for a case on 27 July 2007, but now two cyclones are detected in the analysis window. Figure 14 shows wind fields at the 05Z time slice, which means that the interpolation occurs using SeaWinds satellite data from 00Z and 06Z. The environmental field excludes both cyclones in both original time slices. SeaWinds cyclones are interpolated separately and inserted into the environmental field at the hourly interpolated track position. The resulting blended field for the double-cyclone case is shown in Figure 14C (SW1h). Once again, stencils used in the blending process are shown in Figure 14D.

Further adjustments to the blended database were made by adding QuikSCAT data. Sensitivity tests were made in all cases where this was possible. A discussion section below provides a quantification of number of events throughout the blended database periods when QuikSCAT data was available and inserted to the CFSR-SW1h database. An illustration of the effect of adding QuikSCAT to the blended database is provided in Figure 15, showing the wind speed difference between QuikSCAT and SW1h for the cyclone depicted in Figure 12 for 14 March 2006. It is clear in this case (and most others) that QuikSCAT provides measurements without interpolations that can sharpen and increase the wind intensity in regions that may be critical for wave generation. The latter is explored in more details in Campos et al. (2017).

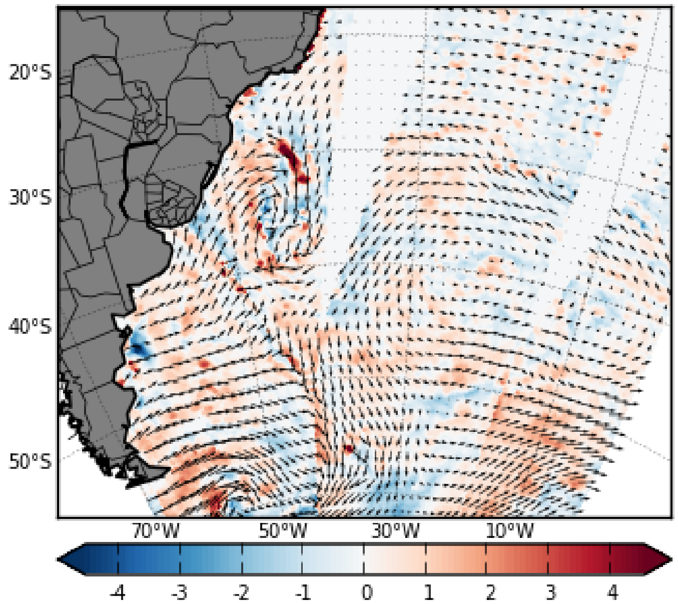

Figure 15 - Differences in wind speed (m/s), QuikSCAT minus SeaWinds, for the cyclone of Figure 12 on 24/03/2006.

Figure 15 shows that QuikSCAT data potentially represent more accurately sharp fronts and higher wind speeds in intense cyclones. Therefore, QuikSCAT winds provide an alternative framework for improving the simulation of extreme waves, in combination with SeaWinds. In the CFSR-satellite set, the blending method within cyclonic areas used QuikSCAT data in directly replacing SW1h winds, for areas and instants where this was applicable. Figure 16 illustrates the process of adding QuikSCAT data to the blended CFSR-SW1h database for an event on 15 June 2008. Stencils on Figure 16D depict the areas where each different wind source was retained, as well as transition zones. Areas with heavy clouds where QuikSCAT flags pointed high uncertainty were excluded; this problem in the QuikSCAT database is discussed by several studies including Freilich and Vanhoff (2006) and Quilfen et al. (2007). Moreover, the few areas with very calm wind conditions inside the cyclone running window did not use satellite data.

Co-located differences, as illustrated in Figure 15, were calculated for all events where scatterometer data was available, leading to the calibration of SW1h winds even for events where no QuikSCAT data was available. This process, which extended the impact of QuikSCAT winds to all cyclonic events in the second blended database, is illustrated in Figure 16. The absence of the orange-color stencil in Figure 16D indicates that no QuikSCAT data is present, i.e, only SeaWinds are used. Nevertheless, a sharper cyclonic wind field is attained due to correction made on the basis of expected biases of SW1h relative to other instances where the latter was co-located with QuikSCAT data.

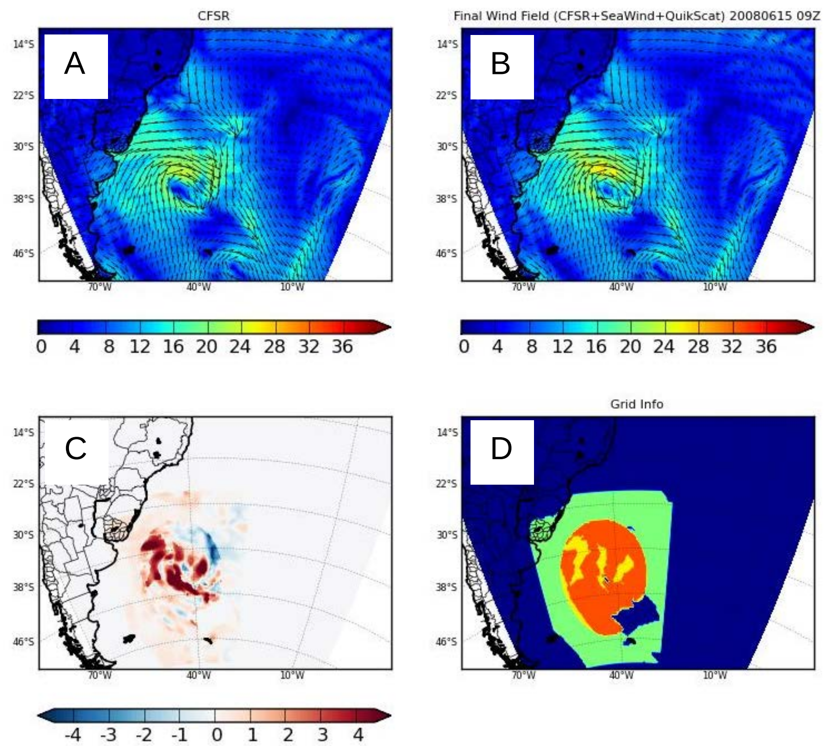

Figure 16 - Example of CFSR cyclonic winds merged with SeaWinds and QuikSCAT data, on 15/06/2008. On the top left (A): original CFSR wind. On the top right (B): Blended wind field with CFSR for non-cyclonic areas and SeaWinds/QuikSCAT inside the cyclone. Bottom left (C): difference between the new blended wind field minus CFSR wind. Bottom right (D): Grid information where in blue is the original CFSR, in dark orange the QuikSCAT wind, in yellow the SeaWinds SW1h and in green the transitioning area.

6. Resulting Surface Wind Datasets

Two classes of wind calibration methods were described in the last section. One is a simple linear regression model applied to CFSR surface winds, with coefficients obtained from the buoy measurements; and the other consists of blending CFSR background winds with cyclonic winds from the SeaWinds database and QuikSCAT. In the latter case, a centered interpolation technique was applied to avoid spatial aliasing of cyclonic wind fields. The application of these approaches separately and in combination, allowed the construction of a set of six alternative wind fields (e.g., Table) that will be described below, and were used as input conditions for WAVEWATCH III wave model simulations detailed discussed elsewhere (e.g., Campos et al., 2017).

Table 4 – Description of the two original winds (CFSR and SeaWinds) and four new wind databases constructed.

CFSR	Original CFSR wind reanalysis
SW	Original SeaWinds satellite database
SW.CI	SeaWinds (SW1h) with cyclones center-interpolated. Final resolution of 1 hour
CFSR.LR	CFSR winds calibrated with linear regression applied to the entire grid and data
CFSR.QsSw	CFSR winds merged with satellite data (QuikSCAT/SeaWinds) within cyclone.
CFSR.LR.QsSw	Combination of CFSR.LR and CFSR.LR.QsSw.

Table 4 summarizes the four newly-constructed wind databases resulting from the current investigation. The sets labeled CFSR and SW are simply the original winds from those two datasets, without any modification. In the case of SeaWinds, sampling was retained at the original 6 h resolution in one of the datasets. The SeaWinds (SW1h) is labeled SW.CI and refers to the original SeaWinds, but with hourly resolution and cyclonic winds redefined by extraction and storm-centered interpolation. CFSR.LR represents the CFSR reanalysis calibrated using the linear regression applied to the entire data. CFSR.QsSw represents the newly-constructed blended wind field, with cyclonic fields in severe storms consisting of a combination of SeaWinds and QuikSCAT data. Finally, CFSR.LR.QsSw represents the combination of CFSR.LR and CFSR.QsSw, where the linear regression is applied to non-cyclonic areas, and the combined satellite winds are inserted within cyclones.

A comparison between alternative surface wind databases is provided in Figure 17. All sets described in Table 4 are illustrated for an event on 27 July 2007, when two intense cyclones co-exist in the South Atlantic Ocean. The general circulation, cyclone position and wind directions are very similar for all alternative wind fields. However, significant differences are seen within the areas of influence of the two cyclones, especially in their north and northwest sectors. In Figure 18, the relative difference between alternative winds is emphasized. The figure uses the original CFSR wind field as the reference and portrays the relative difference constructed winds minus original CFSR. The scale of the color bars are kept the same throughout panels in Figure 18, red colors indicating areas where the new winds are more intense than the original CFSR, and blue colors indicating areas where CFSR is more intense than the constructed winds.

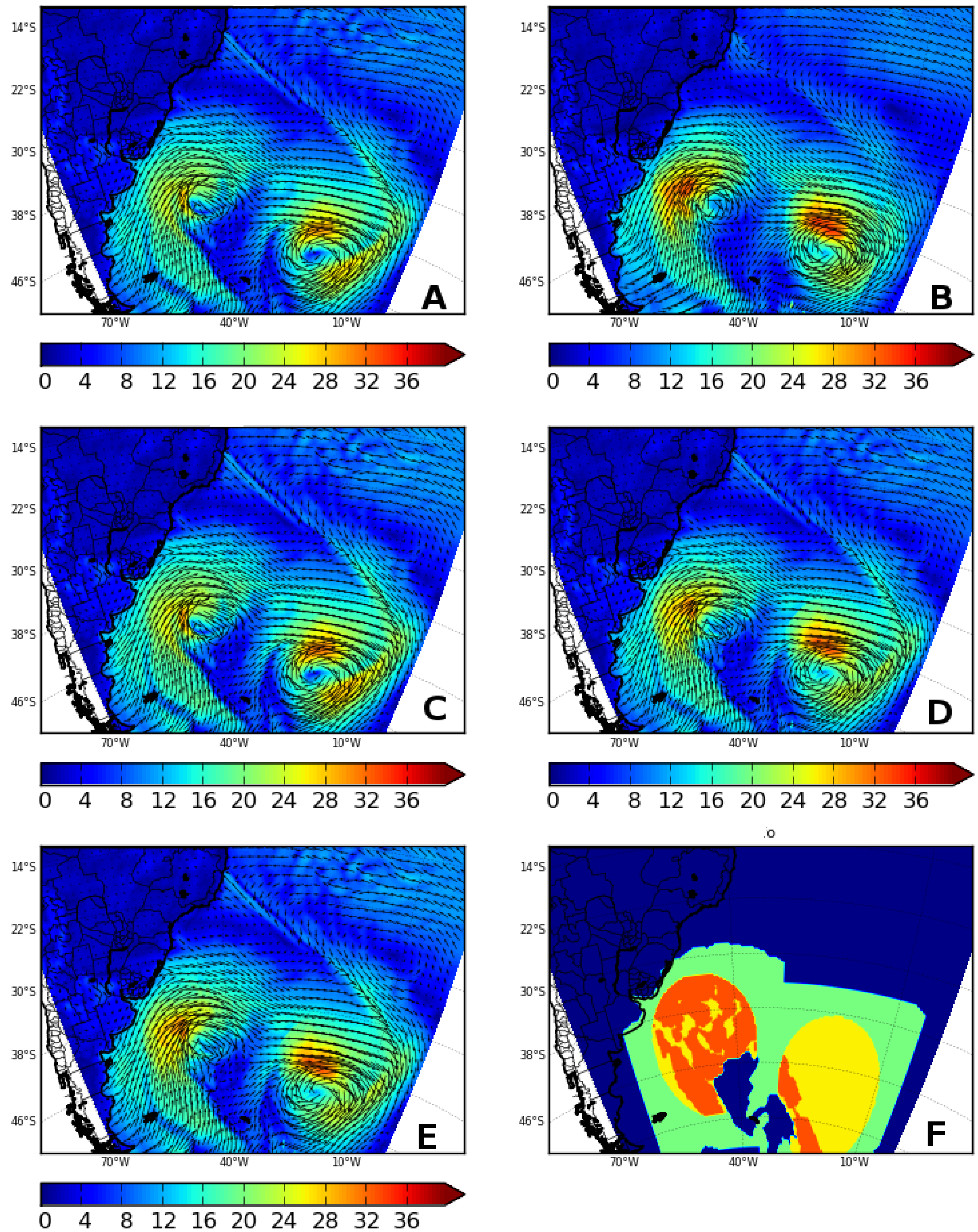

Figure 17 - Surface Winds (m/s) at 09Z on 27/07/2007, same cyclone of Figure 14. A: Original CFSR reanalysis. B: SeaWinds centered interpolated (SW.CI). C: CFSR calibrated using a linear regression function (CFSR.LR). D: CFSR with satellite data inside the cyclones (CFSR.QsSw). E: Composition of D and E, with linear regression applied to the entire CFSR reanalysis apart from the cyclonic areas where satellite is blended (CFSR.LR.QsSw). F: Grid information where in blue is the original CFSR, in yellow the SeaWinds and in green the transitioning area.

Figure 18C shows that the application of the linear regression model has modest overall impact. Small differences are seen between CFSR.LR and the original CFSR, which are proportional to the wind intensity, as described by equation 7. These differences reach up to 2 m/s inside the areas of influence of the two cyclones, but are not restricted to cyclonic areas. Regions with lower wind speeds are less affected relative to the original CFSR.

The largest differences in all data sets are seen in Figure 18B, comparing SeaWinds with CFSR. Within vast patches in the areas of influence of the two cyclones, SeaWinds may be over 4 m/s stronger than CFSR winds, and the underestimation of CFSR is otherwise clearly dominant. Furthermore, some locations in blue indicate that the CFSR data likely overestimates cyclone size, which can be a source of further biases in the estimation of extremes.

Figure 18D shows the effects of blending the SeaWinds-QuikSCAT mix to the CFSR background fields. As expected, areas of influence of the two cyclones have significant differences, and tend to reproduce the behavior seen near cyclones in Figure 18B. Note, however, the finer structure and sharper detail in Figure 18D, relative to panel B, resulting from the inclusion of QuikSCAT cyclonic wind data. Figure 18E illustrates the effects of combining the linear regression model for correcting background CFSR winds, with the blending in of cyclonic winds from satellite measurements.

Combining features of panels C and D, Figure 18E has differences for non-cyclonic areas that are small and have smooth variations, whereas within cyclones the intake of satellite data leads to larger differences. Finally, Figure 18F shows the stencil used in the blending process. Note that the orange stencil clearly depicts a QuikSCAT pass covering a large part of the cyclone on the left, and a small part of the right cyclone, whereas the gaps in cyclonic winds are filled with SeaWinds data (yellow stencil).

A thorough investigation of the impacts of these alternative surface wind field databases to simulations of wind-wave extremes in the South Atlantic Ocean, is provided in a companion paper (Campos et al., 2017), where it is shown that the inclusion of QuikSCAT winds has a decisive impact on improving the agreement of wave hindcasts with upper wave-height percentiles associated with more extreme sea states.

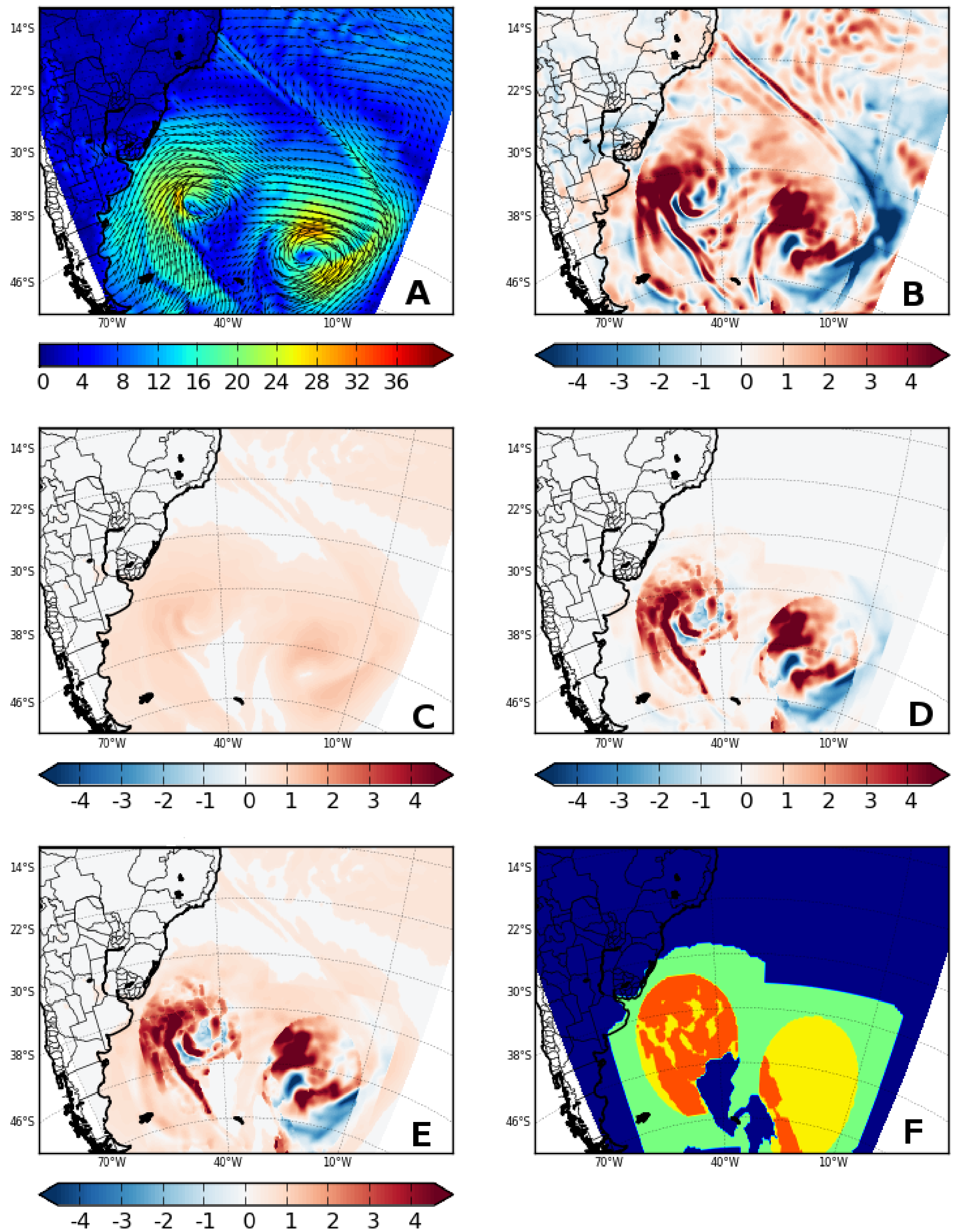

Figure 18 - Surface Wind fields results (m/s) of Figure 19 (09Z on 27/07/2007) compared to original CFSR, taken as the reference. Hot colors in red are the areas where the new wind is more intense than the original CFSR, while cold colors in blue show the areas where the original CFSR is more intense (in m/s). A: Original CFSR wind reanalysis. B: SW.CI minus CFSR. C: CFSR.LR minus CFSR. D: CFSR.QsSw minus CFSR. E: CFSR.LR.QsSw minus CFSR. F: Grid information, where in blue is the original CFSR, in yellow the SeaWinds and in green the transitioning area.

7. Concluding Remarks

The public availability of NCEP's CFSR reanalysis data is an important asset for environmental studies all over the world. Associated with its high accuracy relative to other reanalysis product, this makes this database a powerful tool to improve scientific and technical studies in the oceanic environment. Our study uses the CFSR 10-meters wind fields to investigate its usefulness for driving wind-wave hindcasts, focusing on extreme sea state analysis in the South Atlantic Ocean. An initial evaluation indicates that there are significant CFSR surface wind biases relative to buoy measurements in the South Atlantic, particularly in upper-percentiles, more critical for generating wave hindcasts envisaging extreme analysis.

Two different approaches for calibration of the CFSR data using in situ and remotely-sensed data are presented and compared. One applies a simple linear regression model, with coefficients obtained from the comparison of CFSR against buoy data. In the second, deficiencies of the CFSR winds associated with severe sea state events are remedied, whereby "defective" winds are replaced with satellite data using a Lagrangian approach. The linear regression applied generally increases in around 5% to 6% CFSR wind intensities. However, the process still retains an underestimation by CFSR of up to 25% of remotely-sensed winds within strong extra-tropical storms in the South Atlantic Ocean. Under cyclonic conditions, the proposed method of blending satellite-derived cyclonic wind fields with background CFSR data proves effective, leading to a better representation of winds both during ambient or extreme cyclonic conditions.

A set of six alternative wind data sets is used to force the wave model WAVEWATCH III in a second companion of the present study, where the assessment of results points to a significant advantage of using both CFSR wind adjustment methods, which jointly produce high-quality wind-wave hindcasts for general applications and extreme wave analysis. The current manuscript, focused on a description of CFSR calibration approaches and general validation relative to in situ and remotely-sensed wind measurements, leads to the following conclusions.

- Uncalibrated CFSR winds agree generally well with available Brazilian metocean buoys for calm and moderate intensities. Biases of 0.5 to 1.0 m/s, RMSE between 1 and 2 m/s, and CC around 0.8, suggest that CFSR winds represent well low wind speeds. The quality of CFSR winds degrades with increasing wind intensities. Differences lead to probability density functions with distinct shapes.
- When compared to QuikSCAT data, CFSR winds are relatively lower, particularly near extra-tropical cyclones, where CFSR underestimation is around 5 m/s. This represents relative differences between CFSR and QuikSCAT surface winds of up to 25%. CFSR, SeaWinds and QuikSCAT generally agree in terms of general circulation, cyclone position and wind directions.
- A series of cyclones is identified associated with the occurrence of 47 extreme wave events. Identified cyclone tracks indicate high concentration of cyclones at 40°S of latitude, which show increased wind intensities 48 h before associated extreme wave events, with peak winds occurring 12 h prior to the wave-height peak. Although the cyclone identification is larger around 40°S of latitude, the greatest intensities are found below 40°S.
- In terms of location of cyclonic fetches, there is a persistence of southwesterly winds

offshore the southern Brazil, Uruguay and northeast of Argentina. These regions were identified (Figure 10) as associated with the largest inaccuracies involving extreme waves predicted in the region, highlighting the importance of the implementation of long and continuous measurement campaigns by the local agencies.

- Two methods of wind calibration are investigated to correct CFSR surface wind deficiencies in the South Atlantic. One is a simple linear regression model, and the other uses remotely-sensed data to correct wind speeds within extra-tropical cyclones. Linear regression leads to increasing CFSR winds in 5% to 6% on average, which provides a good calibration for underestimation of moderate winds. Replacement of “defective” winds in cyclones by satellite data provides great improvement to the quality of CFSR winds in areas dominated by severe extra-tropical storm events.

Acknowledgments

This work was funded by Coordenação de Aperfeiçoamento de Pessoal de Nivel Superior (CAPES), a government agency linked to the Brazilian Ministry of Education, under the programme Ciência Sem Fronteiras. Authors would like to acknowledge CAPES as well as the agencies and institutions that provided the data for the present study, namely: National Centers for Environmental Prediction (NCEP/NOAA), National Aeronautics and Space Administration (NASA), National Environmental Satellite, Data, and Information Service (NESDIS/NOAA), National Climatic Data Center (NCDC/NOAA) and the Brazilian Navy with “Programa Nacional de Bóias” (PNBOIA, associated with GOOS-Brazil). The research developed was hosted by two institutions that we are grateful to acknowledge: Environmental Modeling Center (EMC/NCEP/NOAA) and Laboratório de Instrumentaçao Oceanografica of Federal University of Rio de Janeiro (LIOC/PENO/COPPE UFRJ). Finally, we thank the technical support and data from the research center of PETROBRAS (TEO/CENPES/PETROBRAS) and Centro de Hidrografia da Marinha (CHM, Brazilian Navy). The third author holds a visiting position at COPPE/UFRJ, which is funded by Conselho Nacional de Pesquisa of Brazil (CNPq).

References

Alves, J.H.G.M., 1996. Refração do espectro de ondas oceânicas em águas rasas: aplicações a região costeira de São Francisco do Sul, SC. MSc Thesis, UFSC, Florianópolis SC.

Alves, J.H.G.M., Melo, E., 2001. Measurement and modeling of wind waves at the northern coast of Santa Catarina, Brazil. Revista Brasileira de Oceanografia, v.49, n.1-2, São Paulo.

Alves, J.H.G.M., Ribeiro, E.O., Matheson, G.S.G., Lima, J.A.M., Parente, C.E., 2009. Reconstituição do clima de ondas no sul-sudeste brasileiro entre 1997 e 2005. Revista Brasileira de Oceanografia, *27*(3), 427-445, São Paulo.

Alves, J.H.G.M., Chawla, A., Tolman, H.L., Schwab, D., Lang, G., Mann, G., 2014. The Operational Implementation of a Great Lakes Wave Forecasting System at NOAA/NCEP. Weather and Forecasting, v. 29, 1473-1497.

Beu, C.M.L., Ambrizzi, T., 2006, Variabilidade Interanual e Intersazonal da Frequência de Ciclones no Hemisfério Sul. Revista Brasileira de Meteorologia, v. 21 (2), pp. 44-55.

Bitner-Gregersen, E., Bhattacharya, S.K., Cherneva, Z., Dong, S., Fu, T., Kapsenberg, G., Ma, N., Maisondieu, C., Miyake, R., Murphy, A.J., Rychlik, I., Guedes Soares, C. (Ed.) 2015. Proceedings 19th International Ship and Offshore Structures Congress (ISSC 2015) - Committee I.1 Environment Report. Taylor & Francis Group, London, UK. ISBN: 978-1-138-028951.

Caires, S., Sterl, A., 2005. 100-Year Return Value Estimates for Ocean Wind Speed and Significant Wave Height from the ERA-40 Data. Journal of Climate, 18: 1032-1048.

Camargo, R, Harari, J., 1994. Modelagem numérica de ressacas na plataforma sudeste do Brasil a partir de cartas sinóticas de pressão atmosférica na superfície. Bolm Inst. Oceanogr., S Paulo, v. 42(1), p.19-34.

Campos, R. M., 2009, Extreme wave analysis in Rio de Janeiro associated with extra-tropical cyclones over the South Atlantic. MSc. Thesis, COPPE/UFRJ, Rio de Janeiro, RJ, Brazil.

Campos, R.M., Guedes Soarers, C.G., 2016a. Comparison of HIPOCAS and ERA wind and wave reanalyses in the North Atlantic Ocean. Ocean Engineering, v.112, 320–334.

Campos, R.M., Guedes Soarers, C.G., 2016b. Assessment of 3 wind reanalyses in the North Atlantic Ocean. Journal of Operational Oceanography, DOI:10.1080/1755876X.2016.1253328.

Campos, R.M., Guedes Soarers, C.G., 2016c. An hybrid model to forecast significant wave heights. In: Guedes Soares, C., Garbatov, Y., Sutulo, S., Santos, T.A. (Eds.), Maritime Technology Engineering. Taylor & Francis Group, CRC, London, 473–479, ISBN 978-1-138-03000-8, DOI 10.1201/b21890-138. www.crcnetbase.com/doi/pdfplus/10.1201/b21890-138

Campos, R.M., Parente, C.E., Camargo, R., 2012. Extreme wave analysis in Campos Basin (Rio de Janeiro – Brazil) associated with extra-tropical cyclones and anticyclones. Proceedings of the ASME 2012 31st International Conference on Ocean, Offshore and Arctic Engineering, OMAE2012-83117, June 10-15.

Campos, R.M., Camargo, R., Harari, J., 2010. Caracterização de Eventos Extremos do Nível do Mar em Santos e sua Correspondência com as Reanálises do Modelo do NCEP no Sudoeste do Atlântico Sul. Revista Brasileira de Meteorologia, v.25, n.2, 175 - 184.

Campos, R.M., Alves, J.H.G.M., Guedes Soares, C., Guimaraes, L.G. 2017. Extreme Wind-Wave Modeling and Analysis in the South Atlantic Ocean. *Ocean Modelling*, *in press*.

Castro, B.M., Lee, T.N., 1995. Wind-forced sea level variability on the southeast Brazilian shelf. Journal of Geophysical Research, v. 100, n C8, p. 16,045-16,056.

Cavaleri, L, Bertotti, L., 2006. The improvement of modelled wind and wave fields with increasing resolution. Ocean Engineering, v. 33 , 553–565.

Cavaleri, L, Bertotti, L., 2004. Accuracy of the modelled wind and wave fields in enclosed seas. Tellus, 56A, 167–175.

Cavaleri, L., Alves, J.H.G.M., Ardhuin, F., Babanin, A., Banner, M., Belibassakis, K., Benoit, M., Donelan, M., Groeneweg, J., Herbers, T.H.C., Hwang, P., Janssen, P.A.E.M., Janssen, T., Lavrenov, I.V., Magne, R., Monbaliu, J., Onorato, M., Polnikov, V., Resio, D., Rogers, W.E., Sheremet, A., McKee Smith, J., Tolman, H.L., Van Vledder, G., Wolf, J., Young, I., 2007. Progress in Oceanography. 75, 603–674.

Chao, Y.Y., Alves, J.H.G.M., Tolman, H.L., 2005. An Operational System for Predicting Hurricane-Generated Wind Waves in the N Atlantic Ocean. *Weath. & Forecast.*, *20*(4), 652-671.

Chawla, A., Spindler, D.M., Tolman, H.L., 2013. Validation of a thirty year wave hindcast using the climate forecast system reanalysis winds. Ocean Modelling. 70, 189–206.

Dee, D.P., Uppala, S.M., Simmons, A.J., Berrisford, P., Poli, P., Kobayashi, S., Andrae, U., Balmaseda, M.A., Balsamo, G., Bauer, P., Bechtold, P., Beljaars, A.C.M., Van de Berg, L., Bidlot, J., Bormann, N., Delsol, C., Dragani, R., Fuentes, M., Geer, A.J., Haimberger, L., Healy, S.B., Hersbach, H., Hólm, E.V., Isaksen, L., Kållberg, P., Köhler, M., Matricardi, M., McNally, A.P., Monge-Sanz, B.M., Morcrette, J.-J., Park, B.-K., Peubey, C., Rosnay, P., Tavolato, C., Thépaut and, F., Vitart, J.-N., 2011. The ERA-Interim reanalysis: configuration and performance of the data assimilation system. Quart J. R. Meteorol. Soc. 137, 553–597.

Dragani, W.C., Cerne, B.S., Campetella, C.M., Possia, N.E., Campos, M.I., 2013. Synoptic patterns associated with the highest wind-waves at the mouth of the Río de la Plata estuary. Dynamics of Atmospheres and Oceans, 61-62: 1-13.

Freilich, M.H., Vanhoff, B. A., 2006. The accuracy of preliminary WindSat vector wind measurements: Comparisons with NDBC buoys and QuikSCAT, IEEE Trans. Geosci. Remote Sens., 44, 622 – 637.

Gan, M.A., Rao, B.V., 1991. Surface ciclogenesis over South America. Mon. Wea. Rev., v. 119, pp. 293-302.

Gibson, J.K., Kallberg, P., Uppala, S.A, Hernandez, A., Nomura, A., Serrano, E., 1997. ERA description. ECMWF Re-Analysis Project Report Series, Vol. 1, 89 pp.

Godoi, V.A., Parente, C.E., Torres, A.R.T, 2014. An overview of events of high sea waves at the mouth of Guanabara Bay. Pan-American Journal of Aquatic Sciences, v. 9(2), p. 70-87.

Hasselmann, K., Barnett, T.P., Bouws, E., Carlson, H., Cartwright, D.E., Enke, K.,Ewing, J.A., Gienapp, H., Hasselmann, D.E., Krusermann,P., Meerburg, A., Muller, P., Olbers, D.J., Richter, K., Sell, W., Walden, H., 1973. Measurements of wind-wave growth and swell decay during the JointNorth Sea Wave Project (JONSWAP), Ergnzungsheft zur DeutschenHydrographischen Zeitschrift ReiheA8 (Suppl.), 95p.

JPL, 2001: QuikSCAT science data product user's manual (version 2.0). Jet Propulsion Laboratory Publ. D-18053, Pasadena, CA, 84 pp. http://podaac.jpl.nasa.gov/QuikSCAT.

Kalnay, E., Kanamitsu, M., Kistler, R., Collins,W., Deaven, D., Gandin, L., Iredell, M., Saha, S., White, G.,Woollen, J., Zhu, Y., Chelliah, M., Ebisuzaki,W., Higgins,W., Janowiak, J., Mo, K., Ropelewski, C.,Wang, J., Leetmaa, A., Reynolds, R., Jenne, R., Joseph, D., 1996. The NCEP/NCAR reanalysis project. Bul. Am. Meteorol. Soc. 77 (3), 437–471.

Kistler, R., Kalnay, E., Collins, W., Saha, S., White, G., Woollen, J., Chelliah, M., Ebisuzaki, W., Kanamitsu, M., Kousky, V., Van den Dool, H., Jenne, R., Fiorino, M., 2001, The NCEP-NCAR 50-year reanalysis: Monthly means CD-Rom and documentation, BAMS, 82, 247-267.

Kurihara, Y., Bender, M.A., Ross, R.J., 1993. An initialization scheme of hurricane models by vortex specification. Monthly Weather Review, v 121, 2030-2045.

Liu, W.T., Katsaros, K.B., Businger, J.A., 1979. Bulk Parameterizations of Air-Sea Exchanges of Heat and Water Vapor Including Molecular Constraints at the Interface, Journal of Atmospheric Science, Vol. 36, 1722-1735.

Murray, R. J., Simmonds, I., 1991. A numerical scheme for tracking cyclone centers from digital data. Aust. Meteor. Mag., v. 39, pp. 155-166.

Parente, C.E., 1999. Uma Nova Técnica Espectral para Análise Direcional de Ondas. PhD Thesis, COPPE/UFRJ, Rio de Janeiro, RJ, Brazil.

Parente, C. E., Souza, M.H.S., 1989. Wave Climate off Rio de Janeiro. In: Proceedings of 21st Coastal Engineering Conference, Malaga-Spain.

Parente, C.E., Lima, J.A., Violante-Carvalho, N., Assunçao, C.B., 2001. Wave and Wind Extremes Values in Good Weather Situations in the Campos Basin, off Rio de Janeiro. In: Proceedings of 20 th International Conference on Offshore Mechanics and Artic Engineering, OMAE2001, June 3-8.

Pereira Filho, A. J., and R. S. Lima, 2006. Synoptic and mesoscale analysis of hurricane Catarina, Brazil. Proceedings of the 8th International Conf. on Southern Hemisphere Meteorology and Hydrology, Foz do Iguaçu. CDROM, Amer. Meteorol. Soc., Boston, USA.

Pezza, A.B, Simmonds, I., 2006. Catarina: The first South Atlantic hurricane and its association with vertical wind shear and high latitude blocking. In: International Conference on Southern Hemisphere Meteorology and Oceanography (ICSHMO), 8., 2006, Foz do Iguaçu. Proceedings. São José dos Campos: INPE, 2006, p. 353-364. CD-ROM. ISBN 85-17-00023-4.

Pezza, A.B., Ambrizzi, T., 2003. Variability of Southern Hemisphere Cyclone and Anticyclone Behavior: Further Analysis. J. Climate, v. 16, pp. 1075-1083.

Pinho, U.F., 2003, Caracterização dos estados de mar na Bacia de Campos. M.Sc. Thesis, COPPE/UFRJ, Rio de Janeiro, RJ, Brazil.

Powell, M.D., Shirley, M., Dodge, P., Uhlhorn, E., Gamache, J., Cardone, V., Cox, A., Otero, C., Carrasco, N., Annane, B., Fleur, R.S., 2010. Reconstruction of Hurricane Katrina's wind fields for storm surge and wave hindcasting. Journal of Ocean Engineering, 37, pp. 26-36.

Quilfen, Y., Prigent, C., Chapron, B., Mouche, A. A., Houti, N., 2007. The potential of QuikSCAT and WindSat observations for the estimation of sea surface wind vector under severe weather conditions. Journal of Geophysical Research, 112, C09023, doi:10.1029/2007JC004163.

Reboita, M.S., 2008. Ciclones Extratropicais sobre o Atlântico Sul: Simulação Climática e Experimentos de Sensibilidade. PhD Thesis, IAG-USP, São Paulo, SP, Brazil.

Reboita, M. S., Da Rocha, R.P., Ambrizzi, T., Sugahara, S., 2009. South Atlantic Ocean Cyclogenesis Climatology Simulated by Regional Climate Model (RegCM3). Climate

Dynamics, doi:10.1007/s00382-009-0668-7.

Saha, S., Moorthi, S., Pan, H., Wu, X., Wang, J., Nadiga, S., Tripp, P., Kistler, R., Wollen, J., Behringer, D., Liu, H., Stokes, D., Grumbine, R., Gayno, G., Wang, J., Hou, Y., Chuang, H., Juang, H., Sela, J., Iredell, M., Treadon, R., Kleist, D., VanDelst, P., Keyser, D., Derber, J., Ek, M., Meng, J., Wei, H., Yang, R., Lord, S., van den Dool, H., Kumar, A., Wang, W., Long, C., Chelliah, M., Xue, Y., Huang, B., Schemm, J., Ebisuzaki, W., Lin, R., Xie, P., Chen, M., Zhou, S., Higgins, W., Zou, C., Liu, Q., Chen, Y., Han, Y., Cucurull, L., Reynolds, R., Rutledge, G., Goldberg, M., 2010. The NCEP climate forecast system reanalysis. Bull. Am. Meteorol. Soc. 91, 1015–1057.

Silva Dias, P.L., Silva Dias, M.A.F., Seluchi, M., Diniz, F.A., 2004. O Cilclone Catarina: Análise Preliminar da Estrutura, Dinâmica e Previsibilidade. In: XIII Congresso Brasileiro de Meteorologia,2004, 0764: Fortaleza, 10pp.

Souza, M.H.S., 1988. Clima de Ondas ao Norte do Estado do Rio de Janeiro. M.Sc. Thesis, COPPE/UFRJ, Rio de Janeiro, RJ, Brazil.

Stech, J.L., Lorenzzetti, J.A., 1992. The Response of the South Brazil bight to the passage of wintertime cold fronts. Journal of Geophysical Research, v. 97, n. C6, p.9507-9520.

Stopa, J.E., Cheung, K.F., 2014. Intercomparison of wind and wave data from the ECMWF reanalysis Interim and the NCEP climate forecast system reanalysis. Ocean Model. 75, 65–83.

Sugahara, S., 2000. Variacao Anual da Frequencia de Ciclones no Atlantico Sul. XI Congresso Brasileiro de Meteorologia, II Encontro Brasileiro de Interacao Oceano-Atmosfera, Rio de Janeiro, 1: 2607–2611.

Taylor, K.E., 2001. Summarizing multiple aspects of model performance in a single diagram. J. Geophys. Res., 106, 7183-7192.

Tolman, H.L., 1998. Validation of NCEP's ocean winds for the use in wind wave models. Global Atmosphere and Ocean System, 6(3), 243-268.

Tolman, H.L., Alves, J.H.G.M., 2005. Numerical modeling of wind waves generated by tropical cyclones using moving grids. Ocean Modelling , 9 , 305–323.

Tolman, H. L. and the WAVEWATCH III Development Group, 2014. User manual and system documentation of WAVEWATCH III version 4.18. EMC/MMAB/NCEP/NOAA, MMAB Contribution No. 316.

Uppala, S.M., Kållberg, P.W., Simmons, A.J., Andrae, U., da Costa Bechtold, V., Fiorino, M., Gibson, J.K., Haseler, J., Hernandez, A., Kelly, G.A., Li, X., Onogi, K., Saarinen, S., Sokka, N., Allan, R.P., Andersson, E., Arpe, K., Balmaseda, M.A., Beljaars, A.C.M., van de Berg, L., Bidlot, J., Bormann, N., Caires, S., Chevallier, F., Dethof, A., Dragosavac, M., Fisher, M., Fuentes, M., Hagemann, S., Hólm, E., Hoskins, B.J., Isaksen, L., Janssen, P.A.E.M., Jenne, R., McNally, A.P., Mahfouf, J.-F., Morcrette, J.-J., Rayner, N.A., Saunders, R.W., Simon, P., Sterl, A., Trenberth, K.E., Untch, A., Vasiljevic, D., Viterbo, P., Woollen, J., 2005. The ERA-40 re-analysis. Q. J. R. Meteorol Soc., 131; pp. 2961–3012.

Zhang, H., Reynolds, R., Bates, J., 2006. Blended and Gridded High Resolution Global Sea Surface Wind Speed and Climatology from Multiple Satellites: 1987–Present. In: Proceeding of American Meteorological Society 2006 Annual Meeting, Atlanta, GA, America, 29 January–2 February; p.2.23.